

**Toward consistency between trends in bottom-up CO<sub>2</sub> emissions and top-down atmospheric measurements in the Los Angeles megacity**

**S. Newman<sup>1</sup>, X. Xu<sup>2</sup>, K. R. Gurney<sup>3</sup>, Y.-K. Hsu<sup>4</sup>, K.-F. Li<sup>5</sup>, X. Jiang<sup>6</sup>, R. Keeling<sup>7</sup>, S. Feng<sup>8,\*</sup>, D. O'Keefe<sup>3</sup>, R. Patarasuk<sup>3</sup>, K. W. Wong<sup>8</sup>, P. Rao<sup>8</sup>, M. L. Fischer<sup>9</sup>, and Y. L. Yung<sup>1</sup>**

- [1]{Division of Geological and Planetary Sciences, California Institute of Technology, Pasadena, CA 91125, USA}  
[2]{Department of Earth System Science, University of California, Irvine, CA 92697, USA}  
[3]{School of Life Sciences, Arizona State University, Tempe, AZ 85287, USA}  
[4]{Monitoring and Laboratory Division, Air Resources Board, Sacramento, CA 95811, USA}  
[5]{Department of Applied Mathematics, University of Washington, Seattle, WA 98195, USA}  
[6]{Department of Earth and Atmospheric Sciences, University of Houston, Houston, TX 77004, USA}  
[7]{Scripps Institution of Oceanography, University of California, San Diego, La Jolla, CA 92037, USA}  
[8]{Earth Atmospheric Science, Jet Propulsion Laboratory, California Institute of Technology, Pasadena, CA 91109}  
[9]{Environmental Energy Area, E. O. Lawrence Berkeley National Laboratory, Berkeley, CA 94720, USA}  
[\*]{now at Department of Meteorology, Pennsylvania State University, University Park, PA 16802, USA}

Sally Newman 2/18/2016 11:30 PM

Deleted: trends

### 33 Abstract

34 Large urban emissions of greenhouse gases result in large atmospheric  
35 enhancements relative to background that are easily measured. Using CO<sub>2</sub> mole fractions  
36 and  $\Delta^{14}\text{C}$  and  $\delta^{13}\text{C}$  values of CO<sub>2</sub> in the Los Angeles megacity observed in inland  
37 Pasadena (2006-2013) and coastal Palos Verdes peninsula (autumn 2009-2013), we have  
38 determined time series for CO<sub>2</sub> contributions from fossil fuel combustion ( $C_{\text{ff}}$ ) for both  
39 sites and broken those down into contributions from petroleum/gasoline and natural gas  
40 burning for Pasadena. We find a 10 % reduction in Pasadena  $C_{\text{ff}}$  during the Great  
41 Recession of 2008-2010, which is consistent with the bottom-up inventory determined by  
42 the California Air Resources Board. The isotopic variations and total atmospheric CO<sub>2</sub>  
43 from our observations are used to infer seasonality of natural gas and petroleum  
44 combustion. ~~The trend of CO<sub>2</sub> contributions to the atmosphere from natural gas~~  
45 ~~combustion is~~ out of phase with the seasonal cycle of total natural gas combustion  
46 seasonal patterns in bottom-up inventories but ~~is~~ consistent with the seasonality of natural  
47 gas usage by the area's electricity generating power plants. For petroleum, the inferred  
48 seasonality of CO<sub>2</sub> ~~contributions~~ from burning petroleum is delayed by several months  
49 relative to usage indicated by statewide gasoline taxes. Using the high-resolution Hestia-  
50 LA data product to compare  $C_{\text{ff}}$  from parts of the basin sampled by winds at different  
51 times of year, we find that variations in observed fossil fuel CO<sub>2</sub> reflect seasonal  
52 variations in wind direction. The seasonality of the local CO<sub>2</sub> excess from fossil fuel  
53 combustion along the coast, on Palos Verdes peninsula, is higher in fall and winter than  
54 spring and summer, almost completely out of phase with that from Pasadena, also  
55 because of the annual variations of winds in the region. Variations in fossil fuel CO<sub>2</sub>

Sally Newman 2/18/2016 11:36 PM

**Deleted:** For natural gas, inferred emissions

Sally Newman 2/18/2016 11:37 PM

**Deleted:** are

Sally Newman 2/18/2016 11:37 PM

**Deleted:** are

Sally Newman 2/18/2016 11:37 PM

**Deleted:** emissions

Sally Newman 2/19/2016 5:32 PM

**Deleted:** emissions

61 signals are consistent with sampling the bottom-up Hestia-LA fossil CO<sub>2</sub> emissions  
62 product for sub-city source regions in the LA megacity domain when wind directions are  
63 considered.  
64

## 1 Introduction

Carbon dioxide is the most important greenhouse gas (GHG) contributing to current global warming, contributing 64 % of the total radiative forcing, according to the IPCC AR5 report (IPCC, 2013) and comprising 82 % of GHG emissions (NRC, 2010). The global average mole fraction of CO<sub>2</sub> has increased approximately 40 % since pre-industrial times due to anthropogenic emissions (IPCC, 2013). Since the proportion of the world's emissions from megacities (urban regions with more than 10 million inhabitants) is out of proportion with their small surface area (EDGAR, 2009; IEA, 2008), quantifying C<sub>fr</sub> is essential if we are to work aggressively toward their reduction (Duren and Miller, 2012). As a consequence of global warming mitigation, reducing C<sub>fr</sub> could reduce air pollution mortality, which is correlated with increased CO<sub>2</sub> levels (Jacobson, 2008).

Identifying the sources of emissions is a major first step in understanding and mitigating anthropogenic contributions. In cities, especially in megacities, these CO<sub>2</sub> sources often dominate over the normally predominant natural source of the biosphere, at least during certain seasons (e.g., Pataki et al., 2003; Widory and Javoy, 2003; Newman et al., 2013; 2008; Lopez et al., 2013; Turnbull et al., 2011; 2015; Vardag et al., 2015). The most common method of inventorying CO<sub>2</sub> emissions from human activities is through bottom-up reporting by governmental agencies, following IPCC methods (IPCC, 2013). Uncertainties in these methods range from 3-5 % to greater than 50 % (Andres et al., 2012). A more recent, scientifically-based bottom-up approach has been pioneered through the Vulcan and Hestia projects (Gurney et al., 2009; Gurney et al., 2012). These efforts combine multiple streams of data such as air pollution reporting, demographics,

Sally Newman 2/19/2016 5:32 PM

**Deleted:** these emissions

Sally Newman 2/19/2016 5:33 PM

**Deleted:** CO<sub>2</sub> emissions

Sally Newman 2/18/2016 11:38 PM

**Deleted:** This requires self-reporting and may not be reliable in some parts of the world.

property tax data, and traffic monitoring, to arrive at what is proving to be a much more accurate and space/time detailed estimate of fossil fuel CO<sub>2</sub> emissions. The Vulcan Project accomplished fossil fuel CO<sub>2</sub> emission estimation for the whole US at spatial scales of 10 km every hour of the year 2002, with updated years expected by the end of 2015. Hestia is specifically focused on the urban domain and has accomplished estimation down to the individual building and street segment scale for four cities (Indianapolis, IN; Salt Lake City, UT; Los Angeles basin, CA; Phoenix, AZ) with work ongoing in Baltimore, MD (Gurney et al., 2012, Patarasuk et al., in prep.; Rao et al., 2015). Both of these detailed data products are available for selected cities in the United States, facilitating top-down emissions quantification through long-term ambient air monitoring (Duren and Miller, 2012; Gurney et al., 2015). Trends in  $C_{ff}$  must be monitored precisely in order to evaluate progress towards mandated emission reductions. As an example, the California Global Warming Solutions Act of 2006 (Assembly Bill 32) requires reduction of greenhouse gas emissions to 1990 levels by 2020, a reduction of about 15 %. Indeed, now is the time to document the current level of emissions, as governments begin to implement strategies to reduce emissions (e.g., California's Cap-and-Trade Program and Low Carbon Fuel Standards) and want to be able to assess their efficacy.

Within megacities, atmospheric CO<sub>2</sub> concentrations are often highly elevated relative to the regional background due to locally emitted carbon dioxide. This excess can be analyzed for its isotopic composition to help attribute the local emissions to specific processes. Radiocarbon (<sup>14</sup>C) analyses give quantitative information as to the proportions of CO<sub>2</sub> resulting from combustion of ancient sources of carbon (fossil fuels)

Sally Newman 2/19/2016 5:33 PM

Deleted: CO<sub>2</sub> emissions

relative to sources incorporating modern carbon, such as the biosphere (e.g., Levin et al., 2003; Levin and Roedenbeck, 2008; Turnbull et al., 2009), because of its short half-life of 5730 years. The stable isotopes of carbon can be used to separate sources with differing values, such as natural gas and petroleum combustion, with the  $^{13}\text{C}/^{12}\text{C}$  ratio of natural gas typically being lower than that of petroleum (e.g., Keeling, 1961; 1958; Newman et al., 2008; 2013; Pataki et al., 2003; Widory and Javoy, 2003; Djuricin et al., 2010; Moore and Jacobson, 2015), although there can be overlap between petroleum combustion and biological respiration. Therefore, if we know the biosphere's contribution from the fossil fuel  $\text{CO}_2$  contribution derived from  $\Delta^{14}\text{C}$  and the total  $\text{CO}_2$  enhancement over background, we can distinguish all three sources (biosphere, petroleum combustion, and natural gas combustion) provided that there are large variations, such as in urban regions.

Here we report the use of  $^{14}\text{C}$  combined with  $\delta^{13}\text{C}$  in flask samples to disaggregate the local emissions of  $\text{CO}_2$  in the Los Angeles (LA) basin into biosphere, natural gas, and petroleum combustion sources. We investigate the annual patterns and trends for 2006-2013 in these components and compare them to global background and to bottom-up inventories generated by government agencies and scientific colleagues. In particular, we test the method against the changes in  $\text{C}_{\text{ff}}$  observed during and after the Great Recession of 2008-2010 in LA.

The sampling, analytical methods, and calculations are described in section 2. Section 3 discusses the results with regard to spatial and temporal variations and comparison with bottom-up inventories and the detailed data product Hestia-LA. Overall conclusions are presented in section 4.

Sally Newman 2/19/2016 5:34 PM  
**Deleted:** emissions

## **2 Data and analysis**

### **2.1 Locations**

Samples were collected at two locations in the Los Angeles basin: on the campus of the California Institute of Technology (Caltech) in Pasadena, CA ( $34^{\circ}8'12''\text{N}$ ,  $118^{\circ}7'39''\text{W}$ ,  $(240 \pm 5)$  m above sea level), and on Palos Verdes peninsula overlooking the Pacific Ocean and Santa Catalina Island to the south ( $33^{\circ}44.7'\text{N}$ ,  $118^{\circ}20.9'\text{W}$ , 330 m above sea level) (Fig.1). Pasadena is located in the San Gabriel valley, approximately 14 km NE of downtown Los Angeles and 40 km from the coast. Prevailing winds from the SW bring marine air from the ocean during daytime hours, as the planetary boundary layer deepens during heating of the land. During these periods of prevailing south to west winds, the Palos Verdes site is a credible background site. Since the marine air picks up emissions from the basin during its transit inland, Pasadena is a good receptor site for LA emissions. The San Gabriel Mountains just 5 km to the north act as a barrier until midday, when upslope flow and the rising temperature inversion layer allow venting over the mountains (Lu and Turco, 1994; 1995).

### **2.2 Samples**

Air samples were collected into evacuated one-liter Pyrex flasks through Synflex 1300 tubing after passing through  $\text{Mg}(\text{ClO}_4)_2$  to dry the samples. In Pasadena, samples were collected on alternate afternoons at 1400 Pacific Standard Time (PST) using an autosampler, whereas at the Palos Verdes site samples were collected manually once a week (on weekend days) between 1100 and 1600 PST, and typically near 1400 PST. The

163 mid-afternoon sampling time was chosen because this is when the planetary boundary  
164 layer tends to be the deepest and most well mixed during the day. The sampling path at  
165 each location was purged with ambient air before collection.

166 CO<sub>2</sub> was extracted from the air samples cryogenically, following the methods described  
167 in Newman et al. (2008), with the amount of CO<sub>2</sub> determined manometrically. Then the  
168  $\delta^{13}\text{C}$  was determined relative to the Vienna PDB (VPDB) standard (Coplen, 1996) by  
169 dual-inlet isotope ratio mass spectrometry (Thermo-Finnigan MAT 252; Bremen,  
170 Germany) on each individual sample. After this analysis, the CO<sub>2</sub> was frozen into a cold  
171 finger and combined with 3-7 other individual samples to create a composite sample  
172 characterizing mid-afternoon air over a two-week (Pasadena) or month (Palos Verdes)  
173 time period for  $\Delta^{14}\text{C}$  analysis. This differs from the sampling protocol of Affek et al.  
174 (2006), who collected on average two 5-liter samples per month, analyzed each sample  
175 separately, and then averaged the results to produce monthly average  $\Delta^{14}\text{C}$  values for  
176 2004-2005. We found that by combining smaller samples collected more frequently  
177 (alternate days in Pasadena) our results were less scattered than in the previous report and  
178 therefore give interpretable seasonal variations.  $\Delta^{14}\text{C}$  was analyzed by accelerator mass  
179 spectrometer at the Keck-CCAMS facility at the University of California, Irvine, using  
180 the methods described in Newman et al. (2013) and Xu et al. (2007). Analyses of air  
181 from standard tanks calibrated by NOAA (National Oceanic and Atmospheric  
182 Administration) gave errors for CO<sub>2</sub> mole fractions averaging of  $\pm 1.4$  ppm (1 ppm = 1  
183  $\mu\text{mol mol}^{-1}$ ) (n = 44) and  $\delta^{13}\text{C}$  of  $\pm 0.15$  ‰ (n = 30), including extraction, manometry,  
184 and mass spectrometry. Although the uncertainties in the CO<sub>2</sub> mole fractions is much  
185 higher than by spectroscopic techniques, it contributes less than half of the total

Sally Newman 2/22/2016 12:30 PM

Deleted: Pee Dee Belemnite (

Sally Newman 2/22/2016 12:30 PM

Deleted: )

Sally Newman 2/22/2016 12:57 PM

Deleted: Gonfiantini

Sally Newman 2/22/2016 12:58 PM

Deleted: 1978

Sally Newman 2/19/2016 5:34 PM

Deleted: CCMAS



uncertainty in  $C_{ff}$ , which is dominated by the  $\Delta^{14}C$  average error of 2 ‰, based on long-term reproducibility of secondary standards (Xu et al., 2007; Xu et al., 2010; Graven et al., 2013; Miller et al., 2013).

## 2.3 Calculations

A major goal of this study is the attribution of the sources of the  $C_{ff}$  observed. A schematic figure of the flow of data used to calculate the portion of the total  $CO_2$  that is due to biosphere respiration (bio) and fossil fuel (ff) combustion, including burning of petroleum (pet) and natural gas (ng), is shown in Fig. 2. Mole fractions of  $CO_2$  measured at the two sites and a background site in La Jolla, CA, were used to calculate the  $CO_2$  excess (xs) over background (bg). The contributions of fossil fuel combustion and the biosphere to the excess were determined from radiocarbon measurements, and the fossil fuel component was further broken down into petroleum and natural gas using  $\delta^{13}C$  of the  $CO_2$ . Details are described below.

### 2.3.1 Total $CO_2$ emissions and background $CO_2$ mole fraction

The  $CO_2$  excess caused by local emissions at the two sites was calculated by subtracting an estimate of the background  $CO_2$  mole fraction derived from La Jolla monthly values (Keeling et al., 2005; Figs. 3 and 4). Flask sampling at La Jolla is done so as to minimize the influence of local  $CO_2$  sources by sampling during periods that simultaneously satisfy three criteria: low variability in  $CO_2$  concentration for periods of 3 hours or more, wind speed of  $2.6 \text{ m s}^{-1}$  or more from a narrow southwesterly to westerly sector, and high visibility. That these methods successfully minimize influences

Sally Newman 2/19/2016 5:35 PM

Deleted:  $CO_2$  emissions

of local fossil-fuel emissions is indicated by the consistency of the annual radiocarbon concentrations at La Jolla compared to clean stations both to the north and south in the Northern Hemisphere (Graven, 2012). In this paper, therefore, the La Jolla data presented are screened background data. The La Jolla data were interpolated to determine the appropriate value for the midpoint of the range of collection dates included in each  $\Delta^{14}\text{C}$  sample, using the algorithm from Thoning et al. (1989), with two harmonic terms, three polynomial terms, and the smoothed residuals of the long term trend (cutoff of 667 days).

### 2.3.2 $\text{CO}_2$ from fossil fuels, based on $\Delta^{14}\text{C}$

Mass balance calculations were used to calculate the relative contributions of background air, biosphere respiration and photosynthesis, and fossil fuel combustion (including natural gas and oil) to the  $\text{CO}_2$  collected at the two sites. The following equations quantitatively separate the background air, biosphere, and fossil fuel combustion contributions to the locally measured atmospheric  $\text{CO}_2$  using  $\Delta^{14}\text{C}$  (e.g., Levin et al., 2003; Miller et al., 2012; Pataki et al., 2003; Turnbull et al., 2006; Fig. 4):

$$C_{\text{obs}} = C_{\text{bg}} + C_{\text{ff}} + C_{\text{r}} + C_{\text{p}} \quad (1)$$

$$\Delta_{\text{obs}}C_{\text{obs}} = \Delta_{\text{bg}}C_{\text{bg}} + \Delta_{\text{ff}}C_{\text{ff}} + \Delta_{\text{r}}C_{\text{r}} + \Delta_{\text{p}}C_{\text{p}} \quad (2)$$

where subscripts obs, bg, ff, r and p indicate observed, background, fossil fuels, respiration, and photosynthesis, respectively, C indicates  $\text{CO}_2$  mole fraction in ppm, and  $\Delta$  indicates  $\Delta^{14}\text{C}$  in ‰. We assume that  $\Delta_{\text{p}}$  is equivalent to  $\Delta_{\text{bg}}$ , since natural fractionation during uptake is corrected in the  $\Delta^{14}\text{C}$  measurement and therefore substitute

$\Delta_{bg}$  for  $\Delta_p$  in Eq. (2). Then, after solving Eq. (1) for  $C_p$  and substituting this for  $C_p$  in Eq. (2), we solve Eq. (2) for  $C_{ff}$ , resulting in the following expression for  $C_{ff}$ :

$$C_{ff} = \frac{C_{obs}(\Delta_{obs} - \Delta_{bg})}{\Delta_{ff} - \Delta_{bg}} - \frac{C_r(\Delta_r - \Delta_{bg})}{\Delta_{ff} - \Delta_{bg}} \quad (3)$$

The value of  $\Delta_{ff}$  is -1000 ‰, since fossil fuels contain no  $^{14}\text{C}$  because they have been removed from the source of this short-lived radionuclide for millions of years.

We use the record from Pt. Barrow, AK (Xiaomei Xu, unpublished data) for the concurrent background  $\Delta^{14}\text{C}$  values ( $\Delta_{bg}$ ), because [this is the most complete record available for the entire time period of this study. The background  \$\Delta^{14}\text{C}\$  record at Pt. Barrow, AK is obtained through the UCI/NOAA ESRL \(Earth System Research Laboratory\) flask network program that collects whole air samples using 6-L, 1-valve stainless steel canisters \(Silco Can, Restek Co.\) that have been pre-evacuated at UCI. The canisters are pressurized to ~2 atm using an oil-free pump. Two biweekly samples were collected before 2008, and one weekly afterwards. For the period from 17 June 2005 to 17 March 2006, some duplicate samples were collected using 32-L, 1-valve stainless steel canisters. Subsamples were then taken from these samples for  \$^{14}\text{C}\$  analysis.  \$\text{CO}\_2\$  is extracted cryogenically at UCI then converted to graphite by the sealed tube zinc reduction method \(Xu et al. 2007\). Each sample is ~2.7 mg C in size. Analysis of  \$\Delta^{14}\text{C}\$  is performed at the W M Keck AMS facility at UCI with total measurement uncertainty of  \$\pm 1.3\text{--}2.4\text{‰}\$ . Mass dependent fractionation is corrected for using “on-line”  \$\delta^{13}\text{C}\$  measurements during AMS analysis, which accounts for fractionation that occurred during graphitization and inside the AMS. Comparison was made of 22 common sample dates spanning 5 yr, of measured  \$\Delta^{14}\text{C}\$  from Barrow between the UCI and the Scripps Institution of Oceanography’s  \$\text{CO}\_2\$  Program. It shows differences in measured  \$\Delta^{14}\text{C}\$  are](#)

consistent with the reported uncertainties and there is no significant bias between the programs (Graven et al., 2013). Another inter-comparison is that of AMS-based atmospheric  $^{14}\text{CO}_2$  measurements organized by the NOAA Earth System Research Laboratory, Boulder, Colorado. The UCI lab is one the three groups having inter-laboratory comparability within 1‰ for ambient level  $^{14}\text{CO}_2$  (Miller et al. 2013). Comparison of the Pt. Barrow data with those from La Jolla (Graven et al., 2012; Fig. 5) shows good agreement for 2004-2007, when the two data sets overlap. Comparing the calculated values for  $C_{ff}$  from these two backgrounds and propagating through the time series calculations (Section 3.4) results in a difference of approximately 1 % of the signal we are measuring. We calculate  $C_{bio}$  (the sum of  $C_r$  and  $C_p$ ) from Eq. (1), using the calculated values of  $C_{ff}$  and the independent estimates of  $C_{bg}$  from the La Jolla data, so that we understand the contribution of the biosphere to total local emissions.

The nuclear power plant contribution, the only other source of  $^{14}\text{C}$ , is small on the west coast of the U.S. (Graven and Gruber, 2011) and therefore is ignored.

Following Turnbull et al. (2006) and Miller et al. (2012), the respiration terms in the equations above are assumed to reflect contributions due to heterotrophic respiration. Thus, the second term in Eq. (3) is small in magnitude and is due to heterotrophic respiration, through which microbes respire  $\text{CO}_2$  that was from carbon previously incorporated through photosynthesis. This term takes into account the isotopic disequilibrium due to the significant time delay between photosynthetic incorporation and respiration, assumed to be 10 years on average (Miller et al., 2012). The magnitude of this correction for our urban Pasadena site is different relative to sites with smaller anthropogenic  $\text{CO}_2$  signals, since the  $\text{CO}_2$  photosynthesized into the plant a decade ago

was not close to the background air composition of that time but was the local, “polluted” air. The  $\Delta_r$  in Eq. (3) for each sample was calculated by extrapolating the Pasadena trend back 10 years. Because of the mild climate in southern California, we used a constant value of  $C_r = 5$  ppm, the same value used for summer by Turnbull et al. (2006). This should be taken as an upper limit for this urban region. The range of the correction for the second term in Eq. (3), including the sign, was  $-0.06 - -0.11$  ppm, generally smaller relative to regions where the biosphere contribution  $C_r$  is large (Miller et al., 2012; Turnbull et al., 2006). For the data from the Palos Verdes site, we calculated the heterotrophic correction term using values of  $\Delta_r$  calculated by extrapolating the Pt. Barrow background trend back 10 years and used a constant value of  $C_r = 5$  ppm, because of the mild climate. The correction term for the Palos Verdes data ranged from  $0.20 - 0.24$  ppm. The small correction for heterotrophic respiration does not affect any of our conclusions.

In California, there is an added complication when attributing  $\text{CO}_2$  emissions to fossil fuels using  $\Delta^{14}\text{C}$ . Since 2004, 10 % ethanol has been added to gasoline. The ethanol contains modern, not fossil, carbon. For gasoline with 10 % ethanol, 6.7 % of the  $\text{CO}_2$  emitted during combustion is from the modern ethanol (EIA, 2015). A correction for this is made, as discussed in section 2.3.3 below.

### 2.3.3 $\delta^{13}\text{C}$ of $\text{CO}_2$

Plots involving the mole fractions and  $\delta^{13}\text{C}$  can be used to determine  $\delta^{13}\text{C}$  of the local contribution to the observed  $\text{CO}_2$  (Fig. 3). Here we use the Miller-Tans approach (Miller-Tans approach; MT; Miller and Tans, 2003) for this purpose, since it allows for

306 variations in background composition and we observe a widening difference between the  
307 data for  $\delta^{13}\text{C}$  in Pasadena and the La Jolla background record in recent years (Fig. 3e).

308 The following mass balance equations are used in this analysis:

309  $C_{\text{obs}} = C_{\text{bg}} + C_{\text{src}}$  (4)

310  $\delta_{\text{obs}} * C_{\text{obs}} = \delta_{\text{bg}} * C_{\text{bg}} + \delta_{\text{src}} * C_{\text{src}}$  (5)

311 to give

312  $\delta_{\text{obs}} * C_{\text{obs}} - \delta_{\text{bg}} * C_{\text{bg}} = \delta_{\text{src}}(C_{\text{obs}} - C_{\text{bg}})$  (6)

313 (Miller and Tans, 2003), where the subscript src represents the local source of  $\text{CO}_2$   
314 emissions,  $\delta$  represents  $\delta^{13}\text{C}$ , and the appropriate background values are included for  
315 each sample. Using this formulation (Eq. 6), the slope of the correlation (MT slope)  
316 gives the  $\delta^{13}\text{C}$  of this local source. For this analysis, we calculated the MT slopes for  
317 each month and then determined the seasonal averages, averaging December-January-  
318 February as winter, March-April-May as spring, June-July-August as summer, and  
319 September-October-November as autumn. Seven individual samples, over the eight-year  
320 sampling period in Pasadena, were excluded since they fell more than three times the  
321 standard error from their linear regression best-fit lines. The monthly MT plots for 2011  
322 are shown in Fig. A1, as examples. The very high correlation coefficients ( $R = 0.952 -$   
323  $0.999$ ) suggest that  $\delta_{\text{src}}$  remains constant on time scales of a month. We assume that this  
324 is also the case for the isotopic compositions of petroleum and natural gas combustion,  
325 that we describe below.

326 We use the results from the  $^{14}\text{CO}_2$  calculations for the fraction of  $C_{\text{xs}}$  from the  
327 biosphere ( $F_{\text{bio}} = 1 - F_{\text{ff}}$ ) together with the MT slopes to attribute the  $\text{CO}_2$  derived from

petroleum and natural gas combustion ( $C_{\text{pet}}$  and  $C_{\text{ng}}$ ) by mass balance, first by calculating the  $\delta^{13}\text{C}$  of the fossil fuel component, using:

$$\delta_{\text{ff}} = \frac{\delta_{\text{xs}} - \delta_{\text{bio}} * (1 - F_{\text{ff}})}{F_{\text{ff}}} \quad (7)$$

where  $F_{\text{ff}}$  is the fraction of  $C_{\text{xs}}$  due to emissions from fossil fuel combustion, as calculated from the  $^{14}\text{CO}_2$  data. The values for  $\delta_{\text{xs}}$  are the seasonal  $\delta^{13}\text{C}$  values from the MT analyses and  $\delta_{\text{bio}}$  is taken to be -26.6 ‰, the average  $\delta^{13}\text{C}$  of the ambient air plus the discrimination of -16.8 ‰ for the biosphere (Bakwin et al., 1998). This value represents data from temperate northern latitudes (28 – 55 °N), dominated by C3 plants with some C4 grasses present (Bakwin, et al., 1998). Indeed, grasses in southern California are mostly C3 ryegrass, fescue, and bluegrass, with some C4 grasses such as St. Augustine (www.cropsreview.com/c3-plants.html, last accessed January 25, 2016). The proportions of  $\text{CO}_2$  emitted by petroleum and natural gas combustion are calculated using the  $\delta^{13}\text{C}$  values:

$$\delta_{\text{ff}} = F_{\text{pet ff}} * \delta_{\text{pet}} + (1 - F_{\text{pet ff}}) * \delta_{\text{ng}} \quad (8)$$

$$F_{\text{pet ff}} = \frac{\delta_{\text{ff}} - \delta_{\text{ng}}}{\delta_{\text{pet}} - \delta_{\text{ng}}} \quad (9)$$

with an analogous equation for  $F_{\text{ng ff}}$ . where  $F_{\text{pet ff}}$  and  $F_{\text{ng ff}}$  are the fractions of petroleum and natural gas combustion contributions in  $C_{\text{ff}}$ , respectively. The values of  $\delta_{\text{ng}}$  and  $\delta_{\text{pet}}$  used were  $-40.2 \pm 0.5$  ‰ for natural gas (Newman et al., 2008; covering measurements in 1972-1973 and 1999) and  $-25.5 \pm 0.5$  ‰ for petroleum combustion (average of measurements in (Newman et al., 2008; measurements in 2005), and -26.0, -25.1, and -25.5 ‰ measured in 2007, 2012, and 2014, respectively). The  $C_{\text{ff}}$ ,  $C_{\text{pet}}$ , and  $C_{\text{bio}}$  components were corrected for the presence of 10 % ethanol in California gasoline by

350 multiplying  $C_{\text{pet}}$  by 0.067 (the fraction of  $\text{CO}_2$  emitted by burning the ethanol portion of  
351 the ethanol-gasoline mixture; EIA, 2015) to give the amount, in ppm, of  $\text{CO}_2$  that was  
352 included in  $C_{\text{bio}}$  but should have been attributed to  $C_{\text{pet}}$ . The same amount was deducted  
353 from  $C_{\text{bio}}$ . The magnitude of this correction is 0.5 – 1.2 ppm, averaging 0.84 ppm, which  
354 represents approximately a quarter of the  $C_{\text{bio}}$ , but the latter is very small, averaging 3 – 4  
355 ppm and the correction does not affect our results with respect to  $C_{\text{pet}}$  and  $C_{\text{ng}}$ .  
356

#### 357 2.3.4 Time series analysis

358 We used the algorithm of Jiang et al. (2008) to study details of the average annual  
359 patterns of the total  $\text{CO}_2$  and  $C_{\text{ff}}$  in Pasadena, in order to compare with patterns at sites  
360 with less contribution from regional fossil fuel combustion, such as Palos Verdes and La  
361 Jolla background. This method uses the first three Legendre polynomials and harmonic  
362 terms to decompose the signal (Prinn et al., 2000). The harmonic terms define the  
363 seasonal and semi-annual cycles, which we compared to results of the same analysis for  
364 flask data from La Jolla, CA (Keeling et al., 2005).

365 To determine trends in the  $C_{\text{ff}}$  time series, derived from the radiocarbon data, we  
366 used the empirical mode decomposition (EMD) method (Huang et al., 1998; Kobayashi-  
367 Kirschvink et al., 2012). Using this method, nonlinear and nonstationary time series can  
368 be broken down into intrinsic mode functions (IMFs) with increasing period lengths and,  
369 finally, to a long-term trend with at most only one minimum or maximum with slope of  
370 zero. The algorithm involves using cubic splines to calculate maximum and minimum  
371 envelopes for the data series. The average of these envelopes for each time is subtracted  
372 from the original or the previous iteration. This process is repeated until the average is a



horizontal line, giving the first IMF. This IMF is subtracted from the raw time series (or previous starting point) and then repeated until the resulting IMF has only one maximum or minimum in the series, the long-term trend. High frequency modes are removed first, with the earliest representing noise. The later modes are interpreted in terms of known processes, such as annual cycles (e.g., IMFs 3 and 4). Following Wu and Huang (2009), we added random noise equivalent to the error in the measurements to create 300 time series, for which the ensemble EMD (EEMD) analyses were averaged. The EEMD technique is data adaptive, not assuming any shape for the IMFs.

### 3 Results and discussion

The purpose of this project was to determine the sources of  $C_{ff}$  in the Los Angeles basin and compare them with bottom-up inventories and data products from government agencies and the scientific community. Below, we compare results of source allocation from the two sites and then examine the temporal variability at the Pasadena site, with its 8-year record. Then we compare the results with government inventories and with the high-resolution Hestia-LA emissions product.

#### 3.1 Spatial variations – comparison of source attribution at the Pasadena and Palos Verdes sites

The  $\Delta^{14}C$  time series for the two sites are shown in Fig. 3c and d, 8 years for Pasadena and 4 years for Palos Verdes. The two data sets are very different, with Palos Verdes radiocarbon results being significantly higher than those in Pasadena except during the winter. However, the summer months in Pasadena are characterized by  $\Delta^{14}C$  values far from background, i.e., depleted in  $^{14}C$  due to dilution by  $CO_2$  produced by

Sally Newman 2/19/2016 5:36 PM  
Deleted: CO<sub>2</sub> emissions

burning of fossil fuels containing none of the radioactive isotope. There are occasional negative spikes in  $\Delta^{14}\text{C}$  during the winter. Total  $\text{CO}_2$  excess ( $C_{\text{xs}}$ ; Fig. 4), determined as  $\text{CO}_2$  concentration minus background, is similarly disparate with respect to timing. The total enhancement at both Pasadena and Palos Verdes,  $C_{\text{xs}}$ , spikes during winter (up to 65 ppm and 34 ppm, respectively), but the Pasadena excess also peaks during the summer (up to 43 ppm), whereas Palos Verdes values for  $C_{\text{xs}}$  are at a minimum during the warm months (3-20 ppm). When the  $^{14}\text{C}$  and  $C_{\text{xs}}$  information are combined to calculate  $\text{CO}_2$  emissions due to fossil fuels ( $C_{\text{ff}}$ ; eqn. 3; Fig. 4), we see summer maxima for  $C_{\text{ff}}$  in Pasadena, but not in Palos Verdes. The spikes in  $C_{\text{xs}}$  and  $C_{\text{ff}}$  during fall and winter seasons are not the general trend in Pasadena, as evidenced by the quarterly averages (Fig. 6b). The amount of  $C_{\text{ff}}$  in the Pasadena seasonal averages (Fig. 4a, 6b) ranges from  $(18.9 \pm 1.2)$  ppm (winter) to  $(26.8 \pm 0.4)$  ppm (summer). In Palos Verdes,  $C_{\text{ff}}$  averages  $(5 \pm 3)$  ppm during the warmer months and  $(12 \pm 5)$  ppm during the winter months (Fig. 4b). However,  $\text{CO}_2$  emissions from the biosphere ( $C_{\text{bio}}$ ) tend to be higher during the cooler months at both sites (Fig. 4). [Refer to Section 3.2 for more discussion of the biosphere's contribution to  \$C\_{\text{xs}}\$  in Pasadena.](#)

The explanation for the differences in the seasonal cycles of  $C_{\text{xs}}$  and  $C_{\text{ff}}$  at the two sites is probably the different wind patterns for the different times of year. Figure 7 shows back trajectories ending at 1400 PST in Pasadena (Fig. A2 for both sites), calculated using NOAA's HYSPLIT model (Draxler and Rolph, 2014; Rolph, 2014), for January and July 2011. These are representative of these months in all years of this study. Wind directions during July are from the west-southwest, whereas they are mostly from the northeast but much more varied during the winter. Thus, in Pasadena, elevated

$C_{xs}$  and  $C_{ff}$  values during the summer result from air masses traveling across the Los Angeles basin, picking up emissions and transporting them inland. During the winter, the airflow is more mixed, resulting in lower average  $C_{ff}$  signals in Pasadena, since a significant proportion of the winds bring less polluted air from the much less populated mountains and deserts located to the north (Santa Ana winds) (Fig. 7). The summer westerly winds bring ocean air to the Palos Verdes site, characterized by  $CO_2$  mole fractions and  $\Delta^{14}C$  very similar to background marine air. During the cooler months, the Santa Ana winds from the northeast occasionally blow over the LA basin, bringing its emissions to the coastal site (Fig. 7). This pattern results in more scatter in the magnitude of  $CO_2$  excess observed during the winter at the Palos Verdes site, than during the summer. Figure 8 shows the average annual pattern for  $C_{ff}$  at the two sites, demonstrating the effect of the varying wind direction patterns.

### **3.2 Attribution of $CO_2$ excess from different anthropogenic sources for Pasadena**

Since we have information regarding the relative contributions of fossil fuel combustion and biosphere respiration from the radiocarbon data, we can use the differences in the  $\delta^{13}C$  of the  $CO_2$  to look at the contributions of petroleum/gasoline versus natural gas combustion. We use the MT approach to distinguish between different fossil fuel sources of  $CO_2$  (Miller and Tans, 2003). As described in section 2.3.3, the MT slope of the correlation gives the  $\delta^{13}C$  of the local source of  $CO_2$  emissions. In many cases it is difficult to distinguish the anthropogenic sources because the biosphere's signal can overlap that of petroleum. However, in a megacity such as the Los Angeles

basin, the contribution of the biosphere to the total CO<sub>2</sub> enhancement can be minimal (≤20 % in Pasadena; Newman et al., 2008; Newman et al., 2013) during the afternoon, when the boundary layer is deepest and most thoroughly mixed. In this study, we use the information from Δ<sup>14</sup>C presented above to further constrain the biosphere's input. Since the other major anthropogenic sources (cement production and combustion of coal) are not present in the Los Angeles basin, δ<sup>13</sup>C from MT plots can be used to differentiate the proportions of natural gas and oil burned in the region, as discussed below.

Seasonal MT slopes for the mid-afternoon Pasadena samples from 2006 through 2013 are shown in Fig. 6a. We do not present similar analysis for the Palos Verdes data because it is a shorter data set, with only 3-5 measurements per month (12 per season), and the range in CO<sub>2</sub> mole fractions during the warmer months is less than 20 ppm for all spring and summer seasons. Thus there are insufficient meaningful data to produce a significant trend. Vardag et al. (2015) came to this same conclusion for a rural site in Germany, based on a modeling study.

The δ<sup>13</sup>C values from MT regressions for the cooler portions of the year in Pasadena are almost always higher than those for the warmer portions. The values for the cooler seasons average (-30.6 ± 0.5) ‰, 1.8 ‰ higher than the average for the warmer months, (-32.4 ± 0.6) ‰. Assuming that there is no contribution from respiration and that the δ<sup>13</sup>C of the high-CO<sub>2</sub> end members are -40.2 ‰ for natural gas and -25.5 ‰ for petroleum combustion, as discussed above, then the proportion of natural gas burned in C<sub>xs</sub> is 32 % during the cooler months and 45 % during the warmer months. The larger fraction of natural gas burned during the warm part of the year is consistent with the observed burning of more natural gas for electricity generation during summer months, as

Sally Newman 2/19/2016 10:02 AM

**Deleted:** Newman et al. (2008) showed that no biospheric input was required to explain the δ<sup>13</sup>C of mid-afternoon CO<sub>2</sub> during 1972-73 and 2002-2003, although up to 20 % was allowed by the uncertainties.

would be required to power air conditioning needs. Mild winters in this climate require less natural gas combustion for heating buildings, thus minimizing a large winter peak frequently seen in colder regions, such as Salt Lake City, UT (Pataki et al., 2003; Bush et al., 2007) and Chicago, IL (Moore and Jacobson, 2015). This attribution of the different contributions to  $C_{ff}$  still does require knowledge of the  $\delta^{13}C$  value of the biosphere. As mentioned above, we use a discrimination of 16.8 ‰, the average determined by Bakwin et al. (1998) for northern mid-latitudes and includes a mix of C3 and C4 metabolism plants, dominated by C3. More C4 plants will raise the  $C_{ng}$  curve and lower the  $C_{pet}$  curve, since the discrimination by C4 plants is much lower (Farquhar et al., 1989).

As mentioned above, we can use the information provided by the  $^{14}CO_2$  data to put better constraints on contributions from the biosphere. The calculations based on  $\Delta^{14}C$  data in Fig. 6b show that the maximum biosphere contribution was during winter 2012-2013, 7 ppm (28 % of the total  $C_{ff}$ ), and the minimum was 0.1 ppm during spring of 2010. The average is  $(4.1 \pm 0.5)$  ppm (16 % of  $C_{ff}$ ) during cooler months and  $(2.2 \pm 0.3)$  ppm (8 % of  $C_{ff}$ ) during warmer months. The seasonality could be due to variations in emissions from the biosphere. However, it is probably due to a more complex combination of emissions and uptake.

The observation that there are seasonal patterns to the  $CO_2$  emissions from combustion of petroleum and natural gas has implications for the effective composition of  $\Delta^{14}C$  from fuel combustion. The value for fossil fuels is taken to be -1000 ‰, since they contain no  $^{14}C$ . However, because we have 10 % modern ethanol in our gasoline, and there is seasonal variation in the ratio of gasoline to natural gas usage, there is actually a seasonal variation in radiocarbon from the bulk fuel combustion component.

Sally Newman 2/19/2016 10:05 AM

**Deleted:** emissions

Sally Newman 2/19/2016 10:05 AM

**Deleted:** emissions

Sally Newman 2/19/2016 10:05 AM

**Deleted:** emissions

498 And at no time is the  $\Delta^{14}\text{C}$  value actually that of pure fossil fuel (-1000 ‰). The average  
499 value is -954 ‰, and spring-summer periods average 33 ‰ higher than autumn-winter  
500 (-939 – -972 ‰, respectively). These seasonal and overall values for  $\Delta^{14}\text{C}$  of the fuel  
501 component were determined as the best-fit values from the individual  $C_{\text{ff}}$  data to the  
502 seasonal mass balance calculations of  $C_{\text{pet}}$  and  $C_{\text{ng}}$ .

503

### 504 3.3 Average seasonal and semi-annual patterns

505 The emissions of  $\text{CO}_2$  by anthropogenic processes significantly modifies the  
506 annual cycle of  $\text{CO}_2$  observed in the Los Angeles region relative to the oceanic air that  
507 enters the basin, as exemplified by the background air sampled in La Jolla, CA (Keeling  
508 et al., 2005; see discussion in section 2.3.1). There is very little seasonal variability in  
509 Pasadena (Fig. 9a). Whereas the average background annual cycle is characterized by a  
510 peak in April and drawdown in August-September, with an amplitude of 11 ppm (Fig.  
511 9g), the Pasadena cycle is noisy and relatively flat, with lower  $\text{CO}_2$  mole fractions in  
512 January-April and high values the rest of the year and only an amplitude of 5 ppm (Fig.  
513 9a). Each pattern can be modeled well using the Legendre polynomial/harmonic analysis  
514 of Jiang et al. (2008; Fig. 9b, h). The sum of the seasonal and semi-annual harmonic  
515 terms reproduces the data very well, with  $r^2$  values of 0.70 and 0.91 for Pasadena and  
516 background, respectively. The average annual cycles are 6 months out of phase, whereas  
517 the semi-annual oscillation cycles look very similar at the two sites. The seasonal cycle  
518 in Pasadena is consistent with influx of combustion  $\text{CO}_2$  during the hot summer months  
519 due to increased burning of natural gas at power plants located dominantly in the  
520 southwestern portion of the LA basin (CEC, 2015). In contrast, the background data

Sally Newman 2/19/2016 10:08 AM  
Deleted:  $R^2$

reflect global patterns with a drawdown in CO<sub>2</sub> during the summer growing season in the northern hemisphere. Jiang et al. (2012) concluded that the semi-annual oscillation at NOAA's GLOBAL-VIEW sites is due to the combination of gross primary production and respiration of the biosphere. During the winter season, photosynthesis is largely reduced. The peak for gross primary production is relatively flat in winter. However, CO<sub>2</sub> is still emitted to the atmosphere by respiration from the biosphere in winter, which has a relatively sharp peak compared with the photosynthesis term. Thus the combination of gross primary production and respiration leads to the double peaks in each year in the net ecosystem production, which contributes to the semi-annual oscillation in CO<sub>2</sub> (Jiang et al., 2012). The semi-annual oscillation in the background signal is consistent with this interpretation. We see virtually the same pattern in Pasadena, although the amplitude is smaller, consistent with the small biospheric contribution indicated by the  $\Delta^{14}\text{C}$  results.

Based on the work of Jiang et al. (2012) we expect the annual cycle in Pasadena to be larger in amplitude than in La Jolla since it is further north, but the amplitude is actually much smaller. If the regional emissions of CO<sub>2</sub> in Pasadena are relative to a La Jolla background, then there is a huge enhancement during the summer! Indeed, the seasonal cycle for C<sub>fr</sub> (Fig. 8) is 11 ppm, with the peak in August-September, and there is very little semi-annual oscillation.

The annual pattern for CO<sub>2</sub> in Palos Verdes is also heavily influenced by the transport of combustion emissions from the Los Angeles basin (Fig. 7, 8, 9c, d). The average monthly pattern is more similar to the background's (Fig. 9g, h) than to Pasadena's (Fig. 9a, b). However, there is a strong peak in the winter that is consistent

with the increased number of days during this time of year with winds from the north to east, travelling over the basin. Doing the same analysis for the monthly minimum values (Fig. 9e, f) gives a pattern that is much more similar to the background's, confirmed by the comparison of the raw data with the background smoothed time series in Fig. 3. This supports use of minimum values from Palos Verdes as reasonable background for the Los Angeles basin. The  $C_{ff}$  annual pattern is inverse to that in Pasadena, as expected by the seasonal wind patterns (Figs. 7, 8).

The conclusion of this analysis of the annual cycles is that the Pasadena  $CO_2$  pattern is significantly different from the natural cycles observed in La Jolla background and show very little seasonal variation compared with this background. The semi-annual pattern, although smaller in amplitude than expected, is in phase with that observed in the background, which we suggest might reflect a reduced biosphere signature in Pasadena due to artificial irrigation, which may reduce seasonality expected due to wet and dry parts of the year. Both the Pasadena and Palos Verdes average  $CO_2$  patterns reflect the seasonal changes in wind patterns, whereas the monthly minimum Palos Verdes pattern is that expected for the background air entering the LA basin. It will be interesting to see whether water restrictions put into effect during summer of 2015 because of an on-going, severe drought (ca.gov/drought, 2015), affect the patterns observed in the future.

### **3.4 Temporal trends in $CO_2$ excess observed in Pasadena**

#### **3.4.1 Long-term time series analysis**

In order to discern the long-term trends in fossil-fuel  $CO_2$  excess, we must first remove noise and the periodic signals discussed above from the record. We used



569 empirical mode decomposition (EEMD; Huang et al., 1998; Kobayashi-Kirschvink et al.,  
570 2012), as described in the calculation section above, on the 8-year time series of  $C_{ff}$  (Fig.  
571 4a) to identify intrinsic mode functions (IMFs; summary in Fig. 10a-d; full results in Fig.  
572 A3). The noise is represented by the first and second modes (IMF 1 and IMF 2).  
573 Combination of the third and fourth modes of the  $C_{ff}$  time series (IMF 3 and IMF 4)  
574 correlates significantly with the 30-day average record for temperature measured at the  
575 top of the 9-story library next to the sampling site ( $r^2 = 0.6$ ). Note that there are severe  
576 mode mixing problems in IMF3 (e.g. during 2011–2013) between the dominant annual  
577 cycle and subseasonal variations, which also affects the nonlinear decompositions in the  
578 higher modes. To minimize the effects of mode mixing on the extractions of inter-annual  
579 trends, we perform the EEMD again after removing the average annual cycle (minus the  
580 mean of the raw data), defined as monthly averages over the entire time period (2006–  
581 2013; resulting time series shown in Fig. 10e). The revised inter-annual trend is shown in  
582 Fig. 10f. The sum of the trend + IMF 6 is a curve with increasing  $C_{ff}$  values leading up to  
583 mid-2007, when they began to fall, until leveling off in 2010 and perhaps starting to rise  
584 towards the end of the time series. There are end effects in this method, such that we do  
585 not have confidence in the first and last years of the analysis. The uncertainties in this  
586 calculation are shown by the shaded regions in Fig. 10f. These were determined as the  
587  $1\sigma$  standard deviations of adding random noise equivalent to 13.7 % to the data 300 times  
588 and then running the EMD analysis. The 13.7 % noise added is the uncertainty of the  $C_{ff}$   
589 values calculated from  $\Delta^{14}C$ ,  $\pm 1$  ppm, relative to the standard deviation of the data, 7.3  
590 ppm. The maximum and minimum values are distinct at approximately the  $2\sigma$  standard  
591 deviation level, as shown in Fig. 10f and indicate a significant decrease of 9.5 % between

Sally Newman 2/19/2016 10:08 AM  
Deleted: R<sup>2</sup>

the maximum in May 2007, and the average for January-June 2010. Using different backgrounds for  $\Delta^{14}\text{C}$ , such as extrapolating the data from La Jolla (Fig. 5) does not significantly affect this analysis, resulting in differences of  $(0.01 \pm 0.09)$  ppm  $C_{\text{ff}}$  out of a range on the order of 2 ppm. And our result showing that there are different values of  $\Delta^{14}\text{C}$  for bulk fuel for autumn-winter than for spring-summer also does not change these conclusions, since the RMSE of the IMF6+trend (Fig. 10f) using different  $\Delta^{14}\text{C}$  for cool vs. summer months relative to the constant average value is 0.1 ppm  $C_{\text{ff}}$ .

The timing of the drop in the fossil-fuel  $\text{CO}_2$  excess around 2008 is consistent with the economic recession in late 2007-2009 (NBER, 2010) with slow recovery beginning in 2010. Similar results for global  $\text{CO}_2$  emissions due to fossil fuel combustion have been documented by Peters et al. (2012) and Asefi-Najafabady et al. (2014). The fraction of decrease in  $C_{\text{ff}}$  (9.5 %) is similar to, although less than, the decrease in global GDP during this time (global GDP decreased by 13 %; World Bank, 2015).

### 3.4.2 Comparison with inventories and bottom-up gridded $C_{\text{ff}}$ data

A major goal of this study is to compare trends in top-down measurements such as those described here with bottom-up estimates in order to understand how to bring them together in space and time for direct validation. Annual averages of the seasonal amounts derived for  $C_{\text{ff}}$ ,  $C_{\text{pet}}$ , and  $C_{\text{ng}}$  compare well in relative proportions to the averages from California's state inventory provided by the California Air Resources Board (CARB, 2015). Annual values for  $\text{CO}_2$  emissions from all fossil fuels, on-road transportation, and natural gas consumption for the entire state of California, through 2013, are superimposed on the seasonal averages for  $C_{\text{ff}}$ ,  $C_{\text{pet}}$ , and  $C_{\text{ng}}$  in Fig. 11. The

Sally Newman 2/21/2016 11:18 PM

**Deleted:** (average from Fig. 10a plus the maximum in Fig. 10f: 23.7 ppm)

Sally Newman 2/21/2016 11:18 PM

**Deleted:** (average from Fig. 10a plus the average of minimum six-month period from Fig. 10f: 21.4 ppm)

Sally Newman 2/19/2016 5:15 PM

**Deleted:** The observation that  $C_{\text{ff}}$  does not decrease by as large a percentage as the economy is consistent with the analysis of York (2012) that anthropogenic emissions are asymmetric with respect to economic growth and decline. Increases in emissions that come during growth periods are not matched by declines of the same magnitude during economic downturns, because high consumption durable goods that are put in operation during growth remain in use during the decline.

Sally Newman 2/19/2016 5:40 PM

**Deleted: emissions d**

634 decrease in total fossil fuels combustion between 2007 and 2011 in the State's inventory  
635 is 11 %, very similar to the 9.5 % decrease indicated by the EEMD time series analysis of  
636 our  $C_{ff}$  results above. There is a difference in timing between the data presented here  
637 (2010) and those from the CARB inventory (2011-2012) that may be due to uncertainties  
638 in the data or to the different domains covered by the two data sets. The relative  
639 proportions of the on-road portion of the CARB budget is 57 % of fossil fuel  $CO_2$   
640 emissions and the petroleum portion of our top-down estimate averages 54 % of  $C_{ff}$ . This  
641 inventory is for the entire state, not the LA basin, and it includes annual values only.  
642 This discussion has focused on inter-annual variations in  $C_{ff}$ , although, as we have shown  
643 in Fig. 7 and 8, there are at least seasonal variations in wind direction. Looking at back  
644 trajectories from the entire time period of this study, we see no significant shifts in the  
645 winds, from year to year although systematic modeling has not yet been done and is  
646 beyond the scope of this paper. Next, we look at finer spatial and temporal scales.

647 Seasonal variations in  $C_{pet}$  concentration at the Pasadena location can be  
648 compared to the variation in emissions compiled by various sources. Figure 12 presents a  
649 comparison of the  $C_{pet}$  concentration to the petroleum and on-road  $CO_2$  emissions  
650 components estimated by the Energy Information Administration (EIA) (EIA, 2015), the  
651 State of California (CARB, 2015), and the Hestia-LA project (K. R. Gurney, personal  
652 communication). Comparison of the seasonal averages for petroleum consumption data,  
653 based on deliveries (EIA), and gasoline taxes collected (CBE, 2014) with  $C_{pet}$  indicates  
654 similar decreases of 10-20 %, but with a lag of a few months (Fig. 12). The lag could be  
655 due to the different domains of the data sets: EIA and State of California data reflect the

Sally Newman 2/19/2016 5:41 PM

Deleted: emissions

entire state domain while the Hestia  $C_{ff}$  data product reflects the LA Basin specifically, and the atmospheric data presented here represents air sampled in Pasadena.

To truly understand the observations in Pasadena, we must combine information from spatial and temporal meteorological and  $C_{ff}$  databases, such as obtained using a model like the Weather Research and Forecasting (WRF) model. Since this is beyond the scope of this work, we have used the information from HYSPLIT back trajectories (Fig. 7; January and July) to provide rough limits for winds arriving in Pasadena at our sampling time of 14:00 PST. These back trajectories suggest that prevailing winds during the summer come from the southwest, across the basin, and winds during the winter come from the northeast, across the mountains from the desert. We have looked at 1.3-km x 1.3-km gridded  $C_{ff}$  from the Hestia-LA data product to qualitatively determine what relative emissions from petroleum combustion are expected during January and July for the two years of the Hestia data (2011 and 2012). These are plotted in Fig. 12 and agree in seasonality with the observations presented here: more  $C_{pet}$  is observed during the summer than during the winter. A map of the regions selected for January (NE) and July (SW) is presented in Fig. 13a, along with the HYSPLIT back trajectories for January and July, 2011, and the monthly average  $CO_2$  emissions due to total petroleum combustion (the Hestia-LA product) from the two integrated areas based on the wind directions are shown in Fig. 13b for years 2011 and 2012.

We show comparison of the  $C_{ng}$  results from Pasadena with area-integrated bottom-up inventories and the Hestia-LA data product in Fig. 14. The California Energy Commission (CEC, 2015) compiles data for natural gas consumed by power plants throughout the state, including Los Angeles and Orange counties. These seasonal data

Sally Newman 2/19/2016 5:42 PM

**Deleted:** emissions

Sally Newman 2/21/2016 11:42 PM

**Deleted:** Furthermore, the EIA data and the gasoline tax-based data will likely be displaced in space and time from the point of combustion, which is dominated by on-road vehicles. The Hestia data, by contrast, is a fossil fuel  $CO_2$  emissions data product specific in space and time to the individual building and road segments (Gurney et al., 2012).

Sally Newman 2/19/2016 5:43 PM

**Deleted:** emissions

Sally Newman 2/19/2016 5:43 PM

**Deleted:** emissions

691 are consistent with the detailed Hestia-LA data for the electricity production for the entire  
692 Los Angeles basin (dashed dark blue line in Fig. 14a). And the seasonality of all of the  
693 inventories involving just the electrical power sector agrees well with the seasonality of  
694 the time series for  $C_{ng}$  (Fig. 14a), with peaks during the summer and troughs during the  
695 winter. The source attribution analysis using  $\Delta^{14}C$  and  $\delta^{13}C$  also captures the increase in  
696  $C_{ng}$  consumption of the power plants in recent years, although the data from this study  
697 suggest that the increase started earlier than do the inventories. However, the  
698 observations of  $CO_2$  concentration and  $\delta^{13}C$  integrate over all natural gas combustion and  
699 cannot pick out just this one sector.

700 Overall statewide and Los Angeles basin inventories show maximum natural gas  
701 usage during the winter (dashed green line in Fig. 14b). Other sources of combusted  
702 natural gas include residential, commercial, industrial, and transportation use, which  
703 could affect the trends, but we do not have seasonal data for these in the Los Angeles  
704 megacity for the full period of this study. However, the seasonal signal for total  
705 emissions from natural gas combustion from the Hestia-LA project for 2011-2012 is  
706 consistent with the data presented here, when the seasonal prevailing wind directions are  
707 considered. The seasonal pattern of emissions from natural gas combustion at any one  
708 location is characterized by a small peak during the cooler months and a trough during  
709 the warmer months (Fig. 13c). However,  $C_{ff}$  in the region sampled by winds arriving in  
710 Pasadena during the winter (the northeast) are always lower than those in the basin, over  
711 which the summer winds travel to the sampling site. Therefore, transport of air masses  
712 following the seasonal wind patterns can explain the observations in Pasadena. The  
713 earlier onset of the increase in  $C_{ff}$  from natural gas combustion indicated by the data

Sally Newman 2/19/2016 5:43 PM  
**Deleted:** emissions

(2010) relative to that indicated by the government inventories might be due to the mismatch in geographical regions, variations in inter-annual atmospheric transport, or deficiencies in the inventories.

Since the seasonal cycle observed in  $C_{\text{pet}}$  and  $C_{\text{ng}}$  in Pasadena is probably due to atmospheric transport, modeling of this effect is critical to being able to combine top-down observations and bottom-up economic and usage data for a direct consistency comparison. These effects must be removed in order to understand long-term trends due to variations in anthropogenic emissions. The time series analysis using Empirical Mode Decomposition presented in section 3.4.1 removes the seasonal signals to concentrate on the longer-term signals, which show reasonable agreement with the longer-term trends in the statewide inventory.

#### 4 Conclusion

Detection of anthropogenic excess of  $\text{CO}_2$  at two sites in the Los Angeles basin, one on the coast and one inland against a barrier mountain range, reveals significant spatial and seasonal variability due to the biosphere, natural gas combustion, and petroleum combustion. Seasonal patterns in wind direction determine the source region of the excess detected at the two sites. Winds from the west to southwest during the warmer months bring marine air with little excess to Palos Verdes, and these same winds continue across the LA basin picking up emissions from fossil fuel combustion to be observed in Pasadena. During the cooler months, wind directions are more varied and include periods when air with low emissions comes to Pasadena from the northeast to

737 northwest and then travels across the basin to Palos Verdes, incorporating anthropogenic  
738 emissions along the way.

739       The nature of the excess changes with season, as reflected by the  $\delta^{13}\text{C}$  values of  
740  $\text{CO}_2$  observed in Pasadena. During warmer months, lower values for  $\delta^{13}\text{C}$  of the local  
741 excess indicate a higher proportion of natural gas burned, consistent with government  
742 inventories that indicate more natural gas burned during summer to produce electricity to  
743 power air conditioning. Even more importantly, however, the seasonal trends in the  
744 fossil fuel combustion observed in Pasadena are consistent with the shift from  
745 southwesterly winds during warmer months to northeasterly winds during cooler months.  
746 Therefore the source region of emissions changes from the Los Angeles basin during  
747 summer to the mountains and desert during winter, for our Pasadena sampling site.  
748 Trend analysis by ensemble empirical mode decomposition supports the relationship  
749 between emissions and temperature.

750       The long-term trend in  $\text{CO}_2$  excess from fossil fuel combustion is consistent with  
751  $\text{C}_{\text{ff}}$  changes associated with the economic recession and slow recovery of 2008 through  
752 the present, and indicates a significant decrease of 9.5 % since the maximum in late 2007,  
753 consistent with the bottom-up inventory of the California Air Resources Board. Indeed,  
754 top-down and bottom-up methods of determining the anthropogenic sources of  $\text{CO}_2$   
755 emissions must be compared to each other to better understand inconsistencies, potential  
756 biases, and uncertainty. Previously, however, comparisons have been limited by the  
757 scope of emissions, large and overlapping uncertainty, and differences in the target  
758 domain. Here we have shown that combining data from radiocarbon and  $\delta^{13}\text{C}$  values  
759 moves us towards a direct comparison in a megacity with very large emissions.

Sally Newman 2/19/2016 5:44 PM  
**Deleted:** emissions

Measurement trends at a receptor site are consistent with annual variations in California statewide bottom-up inventories for  $C_{ff}$  attributed to petroleum and natural combustion, individually as well as for total CO<sub>2</sub> emissions. Even greater consistency between top-down measurements and granular emission estimates specific for the LA megacity domain are achieved when considering wind direction and sub-city source regions. This strengthens the need to have measurement, modeling, and inventories that are specifically aimed at the same domain with fine space/time resolution.

The next steps are to include modeling with inversion of the measurements to understand the combination of atmospheric transport and emissions and to extend the analysis to a denser network of surface monitoring stations such as the Los Angeles Megacities Carbon Monitoring Project (Kort et al., 2013) and the California Laboratory for Atmospheric Remote Sensing (CLARS) observations from Mount Wilson (Wong et al., 2015). Although the uncertainties are large enough that the method described here will not be usable in non-urban regions, similar to the conclusion of the modeling study by Vardag et al. (2015), anthropogenic  $C_{ff}$  dominate significantly over natural processes in megacities. Therefore, this kind of monitoring in megacities will allow society to understand and monitor the sources of the CO<sub>2</sub> that are the major contributors to global warming.

## Acknowledgments

This work would not have been possible without support from the W.M. Keck Carbon Cycle Facility at UCI. We specifically thank J. Southon for his help with sample analysis. We acknowledge funding from the Keck Institute for Space Studies, NASA Grant NNX13AC04G, and NASA Grant NNX13AK34G. We also acknowledge funding

Sally Newman 2/19/2016 5:45 PM

Deleted: CO<sub>2</sub> emissions

Sally Newman 2/19/2016 5:45 PM

Deleted: emissions



786 from the California Air Resources Board Contract #13-329. The statements and  
787 conclusions in this report are those of the Contract and not necessarily those of the  
788 California Air Resources Board. The mention of commercial products, their source, or  
789 their use in connection with materials reported herein is not to be construed as actual or  
790 implied endorsement of such products. The authors gratefully acknowledge the NOAA  
791 Air Resources Laboratory (ARL) for providing the HYSPLIT transport and dispersion  
792 model used in this publication. We thank N. C. Shu for hosting the site on the Palos  
793 Verdes peninsula.

## 794 References

- 795 [Andres, R. J., Boden, T. A., Bréon, F. M., Ciais, P., Davis, S., Erickson, D., Gregg, J. S.,](#)  
796 [Jacobson, A., Marland, G., Miller, J., Oda, T., Olivier, J. G. J., Raupach, M. R., Rayner,](#)  
797 [P., and Treanton, K.: A synthesis of carbon dioxide emissions from fossil-fuel](#)  
798 [combustion, Biogeosciences, 9\(5\), 1845–1871, doi:10.5194/bg-9-1845-2012, 2012.](#)
- 799 Affek, H. and Eiler, J.: Abundance of mass 47 CO<sub>2</sub> in urban air, car exhaust, and human  
800 breath, *Geochim Cosmochim Acta*, 70(1), 1–12, 2006.
- 801 Asefi-Najafabady, S., Rayner, [P. J.](#), Gurney, [K. R.](#), McRobert, [A.](#), Song, [Y.](#), Coltin, [K.](#),  
802 Huang, [J.](#), Elvidge, [C.](#), and Baugh, [K.](#): A multiyear, global gridded fossil fuel CO<sub>2</sub>  
803 emission data product: Evaluation and analysis of results, *J Geophys. Res-Atmos*, 119,  
804 10,213–10,231, doi:10.1002/2013JD021296, [2014.](#)
- 805 Bakwin, P., Tans, P., White, J. and Andres, R.: Determination of the isotopic (<sup>13</sup>C/<sup>12</sup>C)  
806 discrimination by terrestrial biology from a global network of observations, *Global*  
807 *Biogeochem Cycles*, 12, 555–562, 1998.
- 808 Bush, S., Pataki, D., and Ehleringer, J.: Sources of variation in δ<sup>13</sup>C of fossil fuel  
809 emissions in Salt Lake City, USA, *Appl. Geochem*, 2, 715–723, doi:  
810 10.1016/j.apgeochem.2006.11.001, [2007.](#)
- 811 CARB, California Air Resources Board: available at:  
812 <http://www.arb.ca.gov/cc/inventory/data/data.htm> (last access: July 2015), 2015.
- 813 CBE, California Board of Equalization: available at:  
814 [http://www.boe.ca.gov/sptaxprog/reports/MVF\\_10\\_Year\\_Report.pdf](http://www.boe.ca.gov/sptaxprog/reports/MVF_10_Year_Report.pdf) (last access:  
815 November 2014), 2014.
- 816 CEC, California Energy Commission: available at:  
817 [http://energyalmanac.ca.gov/electricity/web\\_qfer/Power\\_Plant\\_Statistical\\_Information.p](http://energyalmanac.ca.gov/electricity/web_qfer/Power_Plant_Statistical_Information.php)  
818 [hp](#) (last access: January 2015), 2015.
- 819 Clark-Thorne, S. and Yapp, C.: Stable carbon isotope constraints on mixing and mass  
820 balance of CO<sub>2</sub> in an urban atmosphere: Dallas metropolitan area, Texas, USA, *Applied*  
821 *Geochemistry*, 18(1), 75–95, 2003.
- 822 [Coplen, T. B.: Editorial: more uncertainty than necessary, \*Paleoceanography\*, 11, 369–](#)  
823 [370, 1996.](#)
- 824 Djuricin, S., Pataki, D. E. and Xu, X.: A comparison of tracer methods for quantifying  
825 CO<sub>2</sub> sources in an urban region, *J Geophys Res-Atmos*, 115, D11303,  
826 doi:10.1029/2009JD012236, 2010.
- 827 Draxler, R.R. and Rolph: G.D.: HYSPLIT (HYbrid Single-Particle Lagrangian Integrated  
828 Trajectory) Model access via NOAA ARL READY Website  
829 (<http://www.arl.noaa.gov/HYSPLIT.php>). NOAA Air Resources Laboratory, College

830 Park, MD, 2014.  
831  
832 Duren, R. M. and Miller, C. E.: Measuring the carbon emissions of megacities, *Nature*  
833 *Climate Change*, 2(8), 560–562, 2012.

834 EDGAR: European Commission, Joint Research Centre (JRC)/Netherlands  
835 Environmental Assessment Agency (PBL). Emission Database for Global Atmospheric  
836 Research (EDGAR), release version 4.0. <http://edgar.jrc.ec.europa.eu> (last access:  
837 September 2015), 2009.

838 EIA (U.S. Energy Information Agency): Frequently asked questions: available at:  
839 <http://www.eia.gov/tools/faqs/faq.cfm?id=307&t=11>, last access 4 September 2015.

840 Farquhar, G., Ehleringer, J. R., and Hubick, K. T.: Carbon isotope discrimination and  
841 photosynthesis, *Annu. Rev. Plant. Phys. Plant Mol. Biol.*, 40, 503–537, 1989.

842 Graven, H. D., and Gruber, N.: Continental-scale enrichment of atmospheric  $^{14}\text{CO}_2$  from  
843 the nuclear power industry: potential impact on the estimation of fossil fuel-derived  $\text{CO}_2$ ,  
844 *Atmos Chem Phys*, 11, 12339–12349, doi:10.5194/acp-11-12339-2011, 2011.

845 Graven, H. D., Guilderson, T. P. and Keeling, R. F.: Observations of radiocarbon in  $\text{CO}_2$   
846 at La Jolla, California, USA 1992–2007: Analysis of the long-term trend, *J Geophys Res*,  
847 117, D02302, doi:10.1029/2011JD016533, 2012.

848 Graven, H., Xu, X., Guilderson, T. P., and Keeling R. F.: (2013), Comparison of  
849 independent  $\Delta^{14}\text{CO}_2$  records at Point Barrow, Alaska, *Radiocarbon*, 55, 1541–1545,  
850 2013.

851 Gurney, K. R., I. Razlivanov, Y. Song, Y. Zhou, B. Benes, and M. Abdul-Massin:  
852 Quantification of fossil fuel  $\text{CO}_2$  emissions on the building/street scale for a large U.S.  
853 city, *Environ Sci Technol*, 46, 12194–12202, dx.doi.org/10.1021/es3011282, 2012.

854 Gurney, K. R., Romero-Lankao, P., Seto, K. C., Hutyra, L. R., Duren, R., Kennedy, C.,  
855 Grimm, N. B., Ehleringer, J. R., Marcutullio, P., Hughes, S., Pincetl, S., Chester, M. V.,  
856 Runfola, D. M., Feddema, J. J., and Sperling, J.: Climate change: Track urban emissions  
857 on a human scale, *Nature*, 525, 179–181, doi:10.1038/525179a, 2015.

858 Huang, N., Shen, Z. and Long, S.: The empirical mode decomposition and the Hilbert  
859 spectrum for nonlinear and non-stationary time series analysis, *Proc Royal Society*  
860 *London Series A*, 454, 903–995, 1998.

861 IEA: World Energy Outlook 2008, edited by: F. Birol, International Energy Agency.  
862 2008.

863 IPCC: Climate Change 2013: The Physical Science Basis. Contribution of Working  
864 Group I to the Fifth Assessment Report of the Intergovernmental Panel on Climate  
865 Change [Stocker, T.F., D. Qin, G.-K. Plattner, M. Tignor, S.K. Allen, J. Boschung, A.

Sally Newman 2/22/2016 12:59 PM

**Deleted:** Gonfiantini, R.: Standards for stable isotope measurements in natural compounds, *Nature*, 271, 534–536 [online] Available from: <http://www.nature.com/nature/journal/v271/n5645/pdf/271534a0.pdf> (Accessed 12 October 2012), 1978. .

- 873 Nauels, Y. Xia, V. Bex and P.M. Midgley (eds.)). Cambridge University Press,  
874 Cambridge, United Kingdom and New York, NY, USA, 1535 pp., 2013.
- 875 Jacobson, M. Z.: On the causal link between carbon dioxide and air pollution mortality,  
876 *Geophys Res Lett*, 35, L03809, doi:10.1029/2007GL031101, 2008.
- 877 Jiang, X., Li, Q., Liang, M.-C., Shia, R.-L., Chahine, M. T., Olsen, E. T., Chen, L. L. and  
878 Yung, Y. L.: Simulation of upper tropospheric CO<sub>2</sub> from chemistry and transport models,  
879 *Global Biogeochem. Cy.*, 22, GB4025, doi:10.1029/2007GB003049, 2008.
- 880 Jiang, X., Chahine, M. T., Li, Q., Liang, M., Olsen, E. T., Chen, L. L., Wang, J. and  
881 Yung, Y. L.: CO<sub>2</sub> semiannual oscillation in the middle troposphere and at the surface,  
882 *Global Biogeochem. Cy.*, 26, GB3006, doi:10.1029/2011GB004118, 2012.
- 883 Keeling, C.: The concentration and isotopic abundances of carbon dioxide in rural and  
884 marine air, *Geochim Cosmochim Acta*, 24, 277–298, 1961.
- 885 Keeling, C. D.: The concentration and isotopic abundances of atmospheric carbon  
886 dioxide in rural areas, *Geochim Cosmochim Acta*, 13(4), 322–334, doi:10.1016/0016-  
887 7037(58)90033-4, 1958.
- 888 Kobayashi-Kirschvink, K. J., Li, K.-F., Shia, R.-L., and Yung, Y. L., Fundamental modes  
889 of atmospheric CFC-11 from empirical mode decomposition, *Adv Adapt Data Anal*,  
890 04(04), 1250024, doi:10.1142/S1793536912500240, 2012.
- 891 Kort, E. A., Angevine, W., Duren, R., Miller, C. E.: Surface observations for monitoring  
892 urban fossil fuel CO<sub>2</sub> emissions: minimum site location requirements for the Los Angeles  
893 megacity, *J Geophys Res*, 118, 1-8, doi: 10.1002/jgrd.50135, 2013.
- 894 Levin, I. and Roedenbeck, C.: Can the envisaged reductions of fossil fuel CO<sub>2</sub> emissions  
895 be detected by atmospheric observations?, *Naturwissenschaften*, 95, 203–208,  
896 doi:10.1007/s00114-007-0313-4, 2008.
- 897 Levin, I., Kromer, B., Schmidt, M. and Sartorius, H.: A novel approach for independent  
898 budgeting of fossil fuel CO<sub>2</sub> over Europe by <sup>14</sup>CO<sub>2</sub> observations, *Geophys Res Lett*,  
899 30(23), 2194, 2003.
- 900 Lopez, M., Schmidt, M., Delmotte, M., Colomb, A., Gros, V., Janssen, C., Lehman, S. J.,  
901 Mondelain, D., Perrussel, O., Ramonet, M., Xueref-Remy, I. and Bousquet, P.: CO, NO<sub>x</sub>  
902 and <sup>13</sup>CO<sub>2</sub> as tracers for fossil fuel CO<sub>2</sub>: results from a pilot study in Paris during winter  
903 2010, *Atmos Chem Phys*, 13(15), 7343–7358, doi:10.5194/acp-13-7343-2013, 2013.
- 904 Lu, R. and Turco, R.: Air pollutant transport in a coastal environment. Part I: Two-  
905 dimensional simulations of sea-breeze and mountain effects, *Journal of the Atmospheric*  
906 *Sciences*, 51(15), 2285–2308, 1994.
- 907 Lu, R. and Turco, R.: Air pollutant transport in a coastal environment—II. Three-  
908 dimensional simulations over Los Angeles basin, *Atmos Environ*, 29(13), 1499–1518,

909 1995.

910 Miller, J. and Tans, P.: Calculating isotopic fractionation from atmospheric  
 911 measurements at various scales, *Tellus B*, 55, 207–214, 2003.

912 Miller, J. B., Lehman, S. J., Montzka, S. A., Sweeney, C., Miller, B. R., Karion, A.,  
 913 Wolak, C., Dlugokencky, E. J., Southon, J., Turnbull, J. C. and Tans, P. P.: Linking  
 914 emissions of fossil fuel CO<sub>2</sub> and other anthropogenic trace gases using atmospheric  
 915 <sup>14</sup>CO<sub>2</sub>, *J Geophys Res*, 117, D08302, doi:10.1029/2011JD017048, 2012.

916 Miller, J., Lehman, S., Wolak, C., Turnbull, J., Dunn, G., Graven, H., Keeling, R., H.  
 917 Meijer, A., Aerts-Bijma, A. T., and Palstra, S. W.: Initial results of an intercomparison of  
 918 AMS-based atmospheric <sup>14</sup>CO<sub>2</sub> measurements, *Radiocarbon*, 55, 1475–1483, 2013.

919 Moore, J., and Jacobson, A. D.: Seasonally varying contributions to urban CO<sub>2</sub> in the  
 920 Chicago, Illinois, USA region: Insights from a high-resolution CO<sub>2</sub> concentration and  
 921 δ<sup>13</sup>C record, *Elem Sci Anth*, 3, 000052, doi:10.12952/journal.elementa.000052.s004,  
 922 2015.

923 NBER, National Bureau of Economic Research: available at:  
 924 <http://www.nber.org/cycles/sept2010.html> (last access: September 2010), 2010.

925 Newman, S., Xu, X., Affek, H. P., Stolper, E. and Epstein, S.: Changes in mixing ratio  
 926 and isotopic composition of CO<sub>2</sub> in urban air from the Los Angeles basin, California,  
 927 between 1972 and 2003, *J Geophys Res-Atmos*, 113, D23304,  
 928 doi:10.1029/2008JD009999, 2008.

929 Newman, S., Jeong, S., Fischer, M. L., Xu, X., Haman, C. L., Lefter, B., Alvarez, S.,  
 930 Rappenglueck, B., Kort, E. A., Andrews, A. E., Peischl, J., Gurney, K. R., Miller, C. E.  
 931 and Yung, Y. L.: Diurnal tracking of anthropogenic CO<sub>2</sub> emissions in the Los Angeles  
 932 basin megacity during spring 2010, *Atmos Chem Phys*, 13(8), 4359–4372,  
 933 doi:10.5194/acp-13-4359-2013, 2013.

934 NRC, National Research Council: Advancing the Science of Climate Change. National  
 935 Research Council. The National Academies Press, Washington, DC, USA, 2010.

936 Pataki, D., Bowling, D. and Ehleringer, J.: Seasonal cycle of carbon dioxide and its  
 937 isotopic composition in an urban atmosphere: Anthropogenic and biogenic effects, *J*  
 938 *Geophys Res*, 108, 4735, 2003.

939 Patarasuk, R., Gurney, K. R., O'Keefe, D., Song, Y., Huang, J., Rao, P., Buchert, M.,  
 940 Lin, J., Mendoza, D., and Ehleringer, J.: High-resolution fossil fuel CO<sub>2</sub> emissions  
 941 quantification and application to urban climate policy, *Urban Ecosys*, in preparation,  
 942 2015.

943 Peters, G., Marland, G., Le Quéré, C. and Boden, T.: Rapid growth in CO<sub>2</sub> emissions  
 944 after the 2008-2009 global financial crisis, *Nature Climate Change*, 2, 2-4, 2012.

945 Prinn, R. G., Weiss, R. F., Fraser, P. J., Simmonds, P. G., Cunnold, D. M., Alyea, F. N.,  
 946 O'Doherty, S., Salameh, P., Miller, B. R., Huang, J., Wang, R., Hartley, D. E., Harth, C.,  
 947 Steele, L. P., Sturrock, G., Midgley, P. M. and McCulloch, A.: A history of chemically  
 948 and radiatively important gases in air deduced from ALE/GAGE/AGAGE, *J Geophys*  
 949 *Res-Atmos*, 105(D14), 17751–17792, doi:10.1029/2000JD900141, 2000.

950 Rao, P., Gurney, K. R., Patarasuk, R., Song, Y., Miller, C. E., Duren, R. M. Duren, and  
 951 Eldering, A.: Spatio-temporal variations in onroad vehicle fossil fuel CO<sub>2</sub> emissions in  
 952 Los Angeles megacity, *Environ. Sci. Technol.*, submitted, 2015.

953 Rolph, G.D. Real-time Environmental Applications and Display sYstem (READY)  
 954 Website: available at: <http://www.ready.noaa.gov> (last access: July 2015), NOAA Air  
 955 Resources Laboratory, College Park, MD, 2014.

956 Tans, P. P., Berry, J. A. and Keeling, R. F.: Oceanic 13C/ 12C observations: A new  
 957 window on ocean CO<sub>2</sub> uptake, *Global Biogeochem Cycles*, 7(2), 353–368,  
 958 doi:10.1029/93GB00053, 1993.

959 Thoning, K., Tans, P. and Komhyr, W.: Atmospheric carbon dioxide at Mauna Loa  
 960 Observatory, 2, Analysis of the NOAA/GMCC data, 1974-1985, *J Geophys Res*, 94(D6),  
 961 8549–8565, 1989.

962 Turnbull, J., Miller, J., Lehman, S., Tans, P., Sparks, R. and Southon, J.: Comparison of  
 963 <sup>14</sup>CO<sub>2</sub>, CO, and SF<sub>6</sub> as tracers for recently added fossil fuel CO<sub>2</sub> in the atmosphere and  
 964 implications for biological CO<sub>2</sub> exchange, *Geophys Res Lett*, 33, L01817,  
 965 doi:10.1029/2005GL024213, 2006.

966 Turnbull, J., Rayner, P., Miller, J., Naegler, T., Ciais, P. and Cozic, A.: On the use of  
 967 (CO<sub>2</sub>)-C-14 as a tracer for fossil fuel CO<sub>2</sub>: Quantifying uncertainties using an  
 968 atmospheric transport model, *J Geophys Res-Atmos*, 114, D22302,  
 969 doi:10.1029/2009JD012308, 2009.

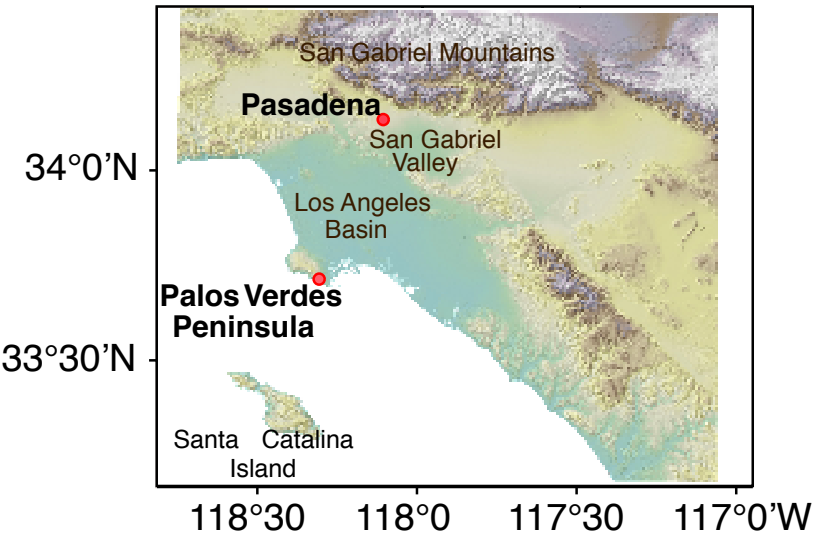
970 Turnbull, J. C., Karion, A., Fischer, M. L., Faloona, I., Guilderson, T., Lehman, S. J.,  
 971 Miller, B. R., Miller, J. B., Montzka, S., Sherwood, T., Saripalli, S., Sweeney, C. and  
 972 Tans, P. P.: Assessment of fossil fuel carbon dioxide and other anthropogenic trace gas  
 973 emissions from airborne measurements over Sacramento, California in spring 2009,  
 974 *Atmos Chem Phys*, 11(2), 705–721, doi:10.5194/acp-11-705-2011, 2011.

975 Turnbull, J. C., Sweeney, C., Karion, A., Newberger, T., Lehman, S. J., Tans, P. P.,  
 976 Davis, K. J., Lauvaux, T., Miles, N. L., Richardson, S. J., Cambaliza, M. O., Shepson, P.  
 977 B., Gurney, K., Patarasuk, R. and Razlivanov, I.: Toward quantification and source sector  
 978 identification of fossil fuel CO<sub>2</sub> emissions from an urban area: Results from the INFLUX  
 979 experiment, *J Geophys Res-Atmos*, 120, 292–312, doi:10.1002/2014JD022555, 2015.

980 Vardag, S. N., C. Gerbig, G. Janssens-Maenhout, and I. Levin: Estimation of continuous  
 981 anthropogenic CO<sub>2</sub> using CO<sub>2</sub>, CO,  $\delta^{13}\text{C}(\text{CO}_2)$  and  $\Delta^{14}\text{C}(\text{CO}_2)$ , *Atmos. Chem. Phys.*  
 982 *Discuss.*, 15(14), 20181–20243, doi:10.5194/acpd-15-20181-2015, 2015.

- 983 Widory, D. and Javoy, M.: The carbon isotope composition of atmospheric CO<sub>2</sub> in Paris,  
984 Earth Planet Sci Lett, 215(1-2), 289–298, 2003.
- 985 Wong, K. W., Fu, D., Pongetti, T. J., Newman, S., Kort, E. A., Duren, R., Hsu, Y.-K.,  
986 Miller, C. E., Yung, Y. L., and Sander, S. P.: Mapping CH<sub>4</sub>:CO<sub>2</sub> ratio in Los Angeles  
987 with CLARS-FTS from Mount Wilson, Atmos Chem Phys, 15, 241-252, 2015.
- 988 World Bank: GDP,  
989 [http://data.worldbank.org/indicator/NY.GDP.MKTP.CD/countries/1W-US?](http://data.worldbank.org/indicator/NY.GDP.MKTP.CD/countries/1W-US?display=graph)  
990 [display=graph](http://data.worldbank.org/indicator/NY.GDP.MKTP.CD/countries/1W-US?display=graph), last access: May 2015.
- 991 Wu, Z. and Huang, N. E.: Ensemble empirical mode decomposition: A noise-assisted  
992 data analysis method, Adv Adapt Data Anal, 1(01), 1–41, 2009.
- 993 Xu, X., Trumbore, S. E., Zheng, S., Southon, J. R., McDuffee, K. E., Luttgen, M. and  
994 Liu, J. C.: Modifying a sealed tube zinc reduction method for preparation of AMS  
995 graphite targets: Reducing background and attaining high precision, Nucl Instrum Meth  
996 B, 259, 320–329, 2007.
- 997 [Xu, X., Khosh, M. S., Druffel-Rodriguez, K. C., Trumbore S. E., and Southon J. R.:  
998 \(2010\). Is the consensus value of ANU sucrose \(IAEA C-6\) too high? Radiocarbon, 52,  
999 866-874, 2010.](#)
- 1000 York, R.: Asymmetric effects of economic growth and decline on CO<sub>2</sub> emissions, Nature  
1001 Climate Change, 2(11), 762–764, doi:10.1038/nclimate1699, 2012.

1002 **FIGURES**



1003 Figure 1. Map of southern California, showing sampling locations in Pasadena and Palos  
1004 Verdes (red dots).



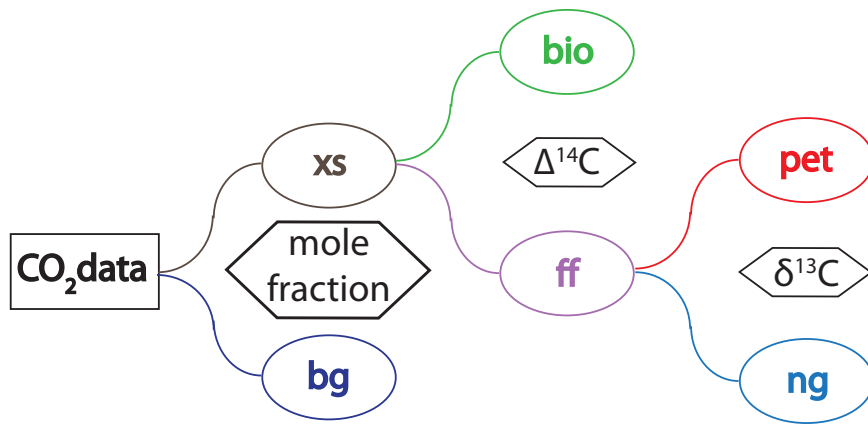


Figure 2. Schematic diagram showing the use of different data sets for attribution of the sources of CO<sub>2</sub> emissions. Mole fractions of background (bg) and observations are used to determine C<sub>xs</sub> (excess over background/bg); Δ<sup>14</sup>C values are used to distinguish C<sub>ff</sub> (fossil fuel, ff) and C<sub>bio</sub> (biosphere, bio); δ<sup>13</sup>C compositions are used to distinguish C<sub>pet</sub> (petroleum/gasoline, pet) from C<sub>ng</sub> (natural gas, ng).

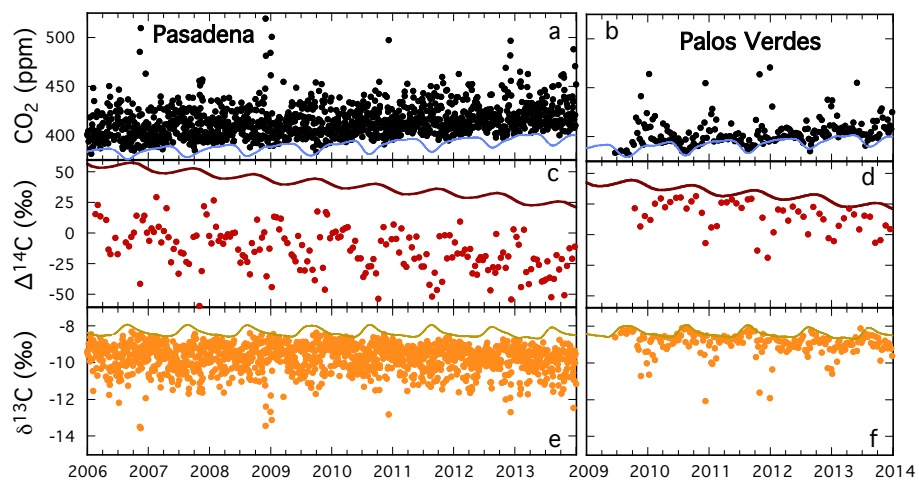
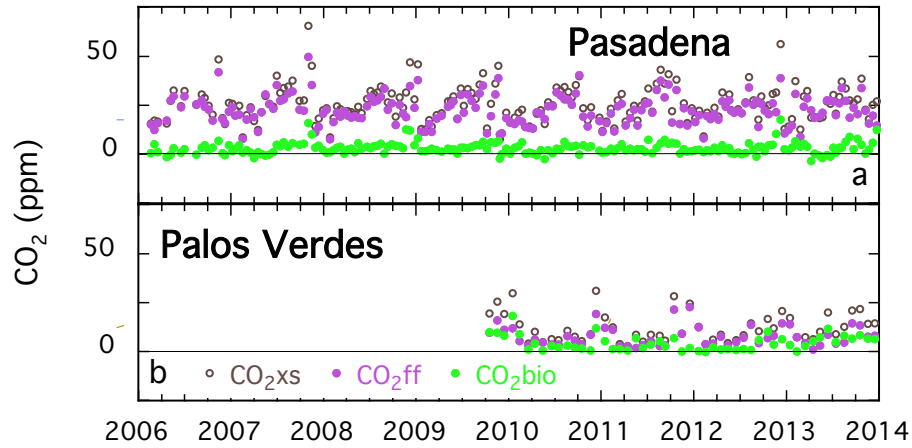
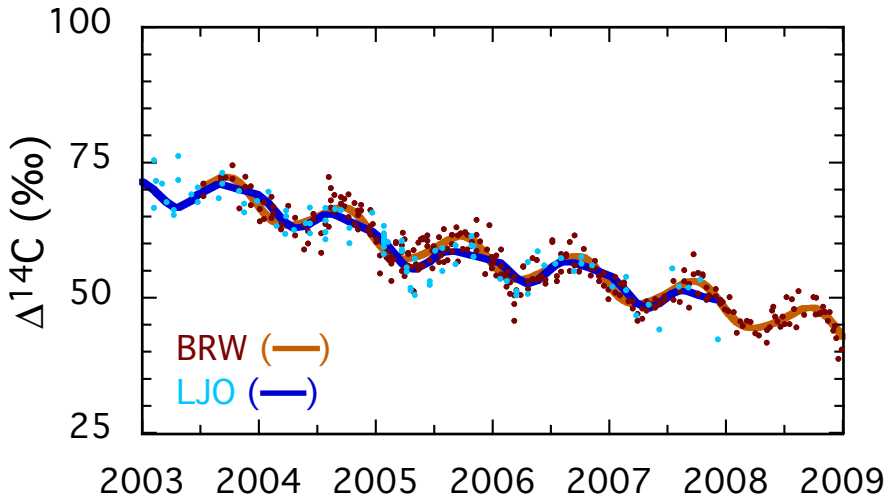


Figure 3. Time series of CO<sub>2</sub> mole fractions for <sup>14</sup>CO<sub>2</sub> samples (a, b), Δ<sup>14</sup>C data (c, d), and δ<sup>13</sup>C (e, f) for Pasadena and Palos Verdes. The solid curves are backgrounds used in the calculations: δ<sup>13</sup>C and CO<sub>2</sub> backgrounds are from La Jolla, CA and Δ<sup>14</sup>C from Pt. Barrow, AK.



1014 Figure 4. Time series of  $C_{xs}$ ,  $C_{ff}$ , and  $C_{bio}$  calculated from  $\Delta^{14}C$  (see text for description of  
 1015 calculations) for Pasadena (a) and Palos Verdes (b). The errors for  $C_{ff}$  are 1 ppm. The  
 1016 negative  $C_{bio}$  values indicate photosynthetic uptake. The value of  $\Delta^{14}C$  for fuel for this  
 1017 calculation was taken to be -954 ‰, the average from the summer and winter  
 1018 calculations.



1019 Figure 5. Comparison of possible background records for this study, Pt. Barrow, AK,  
 1020 (BRW; Xiaomei Xu, unpublished data) and La Jolla, CA (LJO; Graven et al., 2012). The  
 1021 smoothed brown curve for BRW is the  $\Delta^{14}\text{C}$  background used for this study and was  
 1022 calculated using the algorithm of Thoning et al. (1989), from the function plus the  
 1023 smoothed residuals of the long-term trend, using 2 harmonic and 3 polynomial terms in  
 1024 the function and 667 days as the long-term cutoff for the low-pass filter.

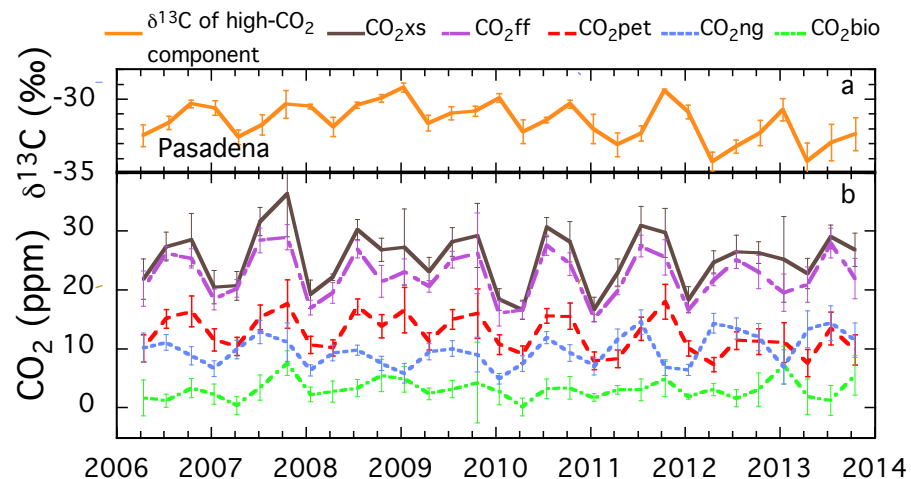


Figure 6. Attribution of  $\text{CO}_2$  excess in Pasadena among combustion of natural gas and petroleum and the biosphere. (a) Miller-Tans slopes for seasonal averages of monthly plots. Error bars are standard errors of the regression intercepts. (b) Attribution of  $\text{C}_{\text{xs}}$  among all three sources (natural gas, petroleum, and the biosphere), combining the information from  $\Delta^{14}\text{C}$  and  $\delta^{13}\text{C}$ , using Miller-Tans slopes to determine the relative proportions of petroleum and natural gas combustion. Error bars are propagated from the errors in the  $\delta^{13}\text{C}$  intercepts and the  $\Delta^{14}\text{C}$  measurements.

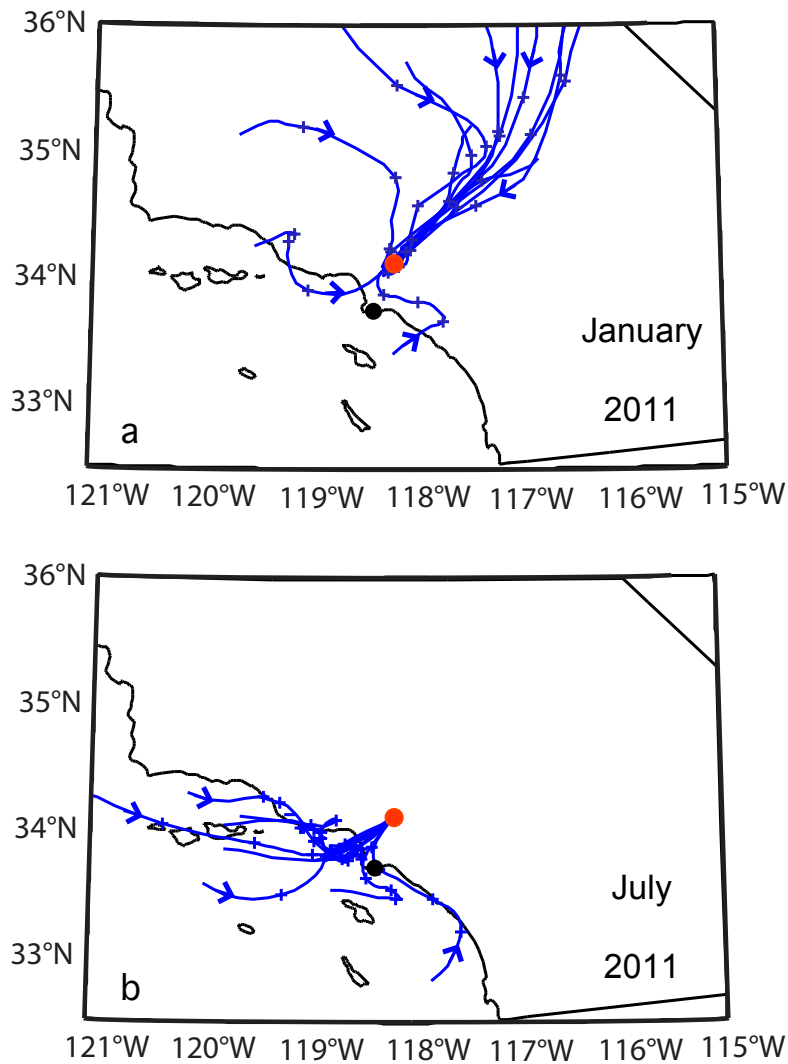
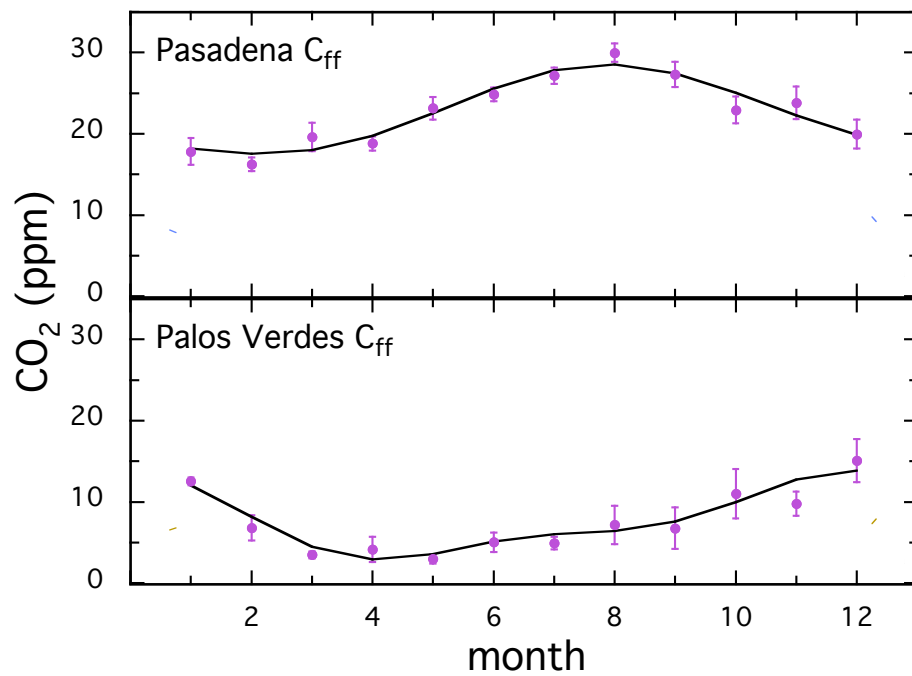


Figure 7. Back trajectories (24 hour) for winds arriving at the Pasadena site (red dot) at 1400 PST for January (a) and July (b) 2011, calculated by HYSPLIT (Draxler and Rolph, 2015; Rolph, 2015) for all sampling days in January and selected sampling days in July, for clarity. Results for all sampling days are shown in Fig. A2. Arrows indicate the direction of air flow. Plus signs indicate 6, 12, and 18 hours from the Pasadena site. The black dot is the location of the Palos Verdes site. The back trajectories for the Palos Verdes site show a similar pattern (Appendix Fig. A2). The back trajectories explain the difference between the annual cycles at the two sites, shown in Fig. 8.



1040 Figure 8. The annual patterns for  $C_{ff}$  in Pasadena and Palos Verdes calculated as the best  
 1041 fit of two harmonics plus the average of the annual cycles (black curves). These patterns  
 1042 are consistent with seasonal differences in the back trajectories shown in Fig. 7.

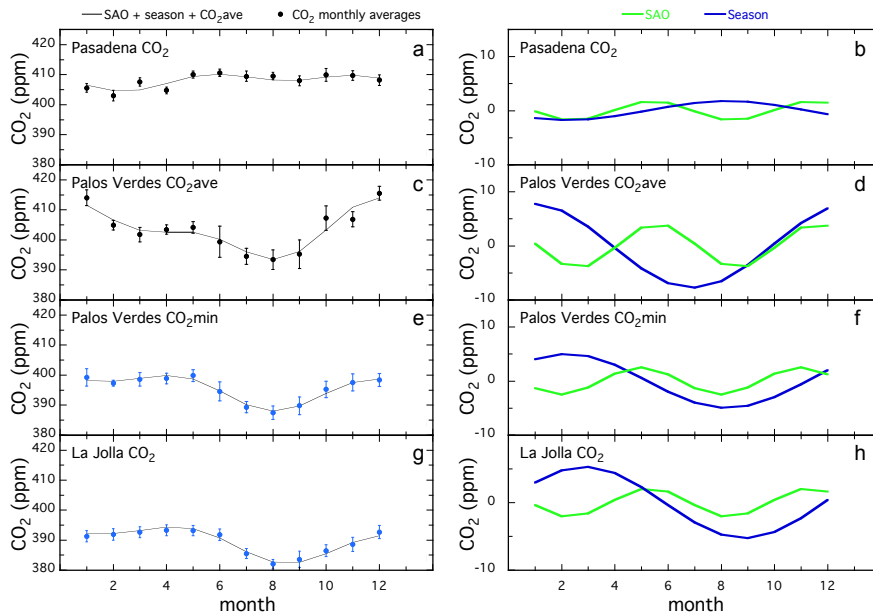


Figure 9. Comparison of seasonal and semi-annual oscillation cycles of CO<sub>2</sub> mole fractions for flask samples from Pasadena (2006-2013) with those at the La Jolla (2006-2013) and Palos Verdes (2009-2013) sites. Left column panels show the average annual patterns for the monthly averages together with the sum of the harmonics for seasonal (blue) and semi-annual (green) cycles (Jiang et al., 2008). Right column panels show the amplitudes and phases of the pure harmonic components. Two sets of results are shown for Palos Verdes, for the monthly averages (c, d) and for the monthly averages of weekly minima (e, f). The monthly averages show the effect of transport on the signal, with a large peak during the winter, while the minima (in blue) show that data from this site are very similar to La Jolla (in blue) and should be a good estimation of the background air for the LA basin. Error bars on the monthly averages of the data are  $1\sigma$  standard errors.



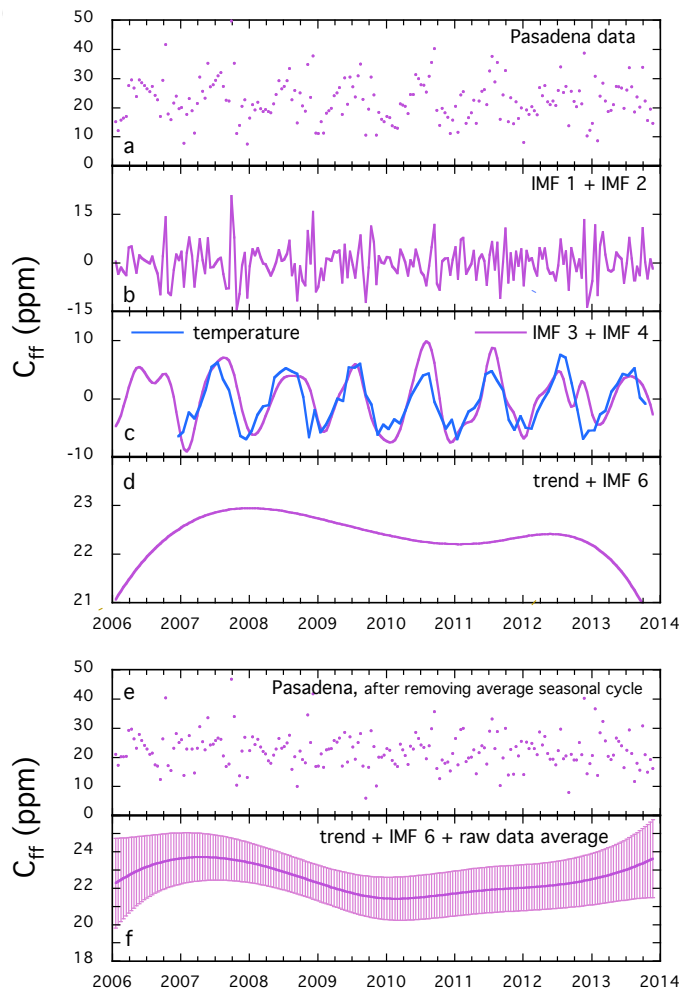


Figure 10. Results of ensemble empirical mode decomposition (EEMD) (Huang et al., 1998; Wu and Huang, 2009) of the  $C_{ff}$  time series calculated using Eq. (3) and the average, constant  $\Delta^{14}C$  of -954 ‰ for fossil fuel. The top set of panels show the raw data (a), noise (b), annual and semi-annual mode (c), and the trend + IMF 6 (d). The pattern of the trend + IMF 6 shown in (d) is within  $1\sigma$  uncertainty of no variation over this time period. The bottom two panels include the raw data after subtracting the average annual cycle (centered at zero) (e) and the trend + IMF 6 for the modified data set (f). 30-day average temperatures (minus the overall average and scaled to match the magnitude of the  $C_{ff}$  IMF; blue curve) are superimposed on the plot of IMF 3 + IMF 4 (c). Shaded regions in (f) indicate  $1\sigma$  standard deviation of 300 Monte Carlo realizations with 13.7 % noise added, the ratio of the uncertainty in  $C_{ff}$  to the standard deviation of the data.

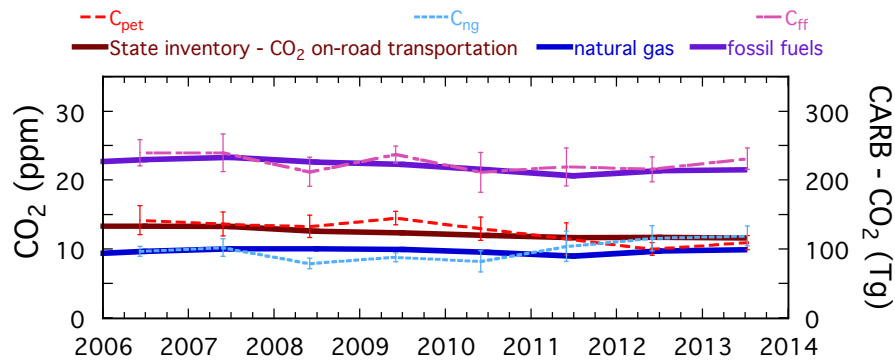


Figure 11. Comparison of annual average CO<sub>2</sub> emissions from bottom-up California Air Resources Board (CARB) inventories (thick lines; right axis labels) for fossil fuel-derived emissions with top-down annual averages from the Pasadena data, using the Miller and Tans (2003) approach to attribute CO<sub>2</sub> emissions from petroleum and natural gas combustion from the  $\delta^{13}\text{C}$  measurements. Annual curves showing the attribution of  $C_{\text{xs}}$  averaged from the seasonal values from Fig. 6b are shown as thinner lines. The error bars on the results from the flask sample data are 1 $\sigma$  standard errors of the means. The annual trends from the bottom-up CARB inventories are plotted on a scale exactly 100 times that of the trends derived from the CO<sub>2</sub> measurements, showing that the relative proportions are very similar through 2013.

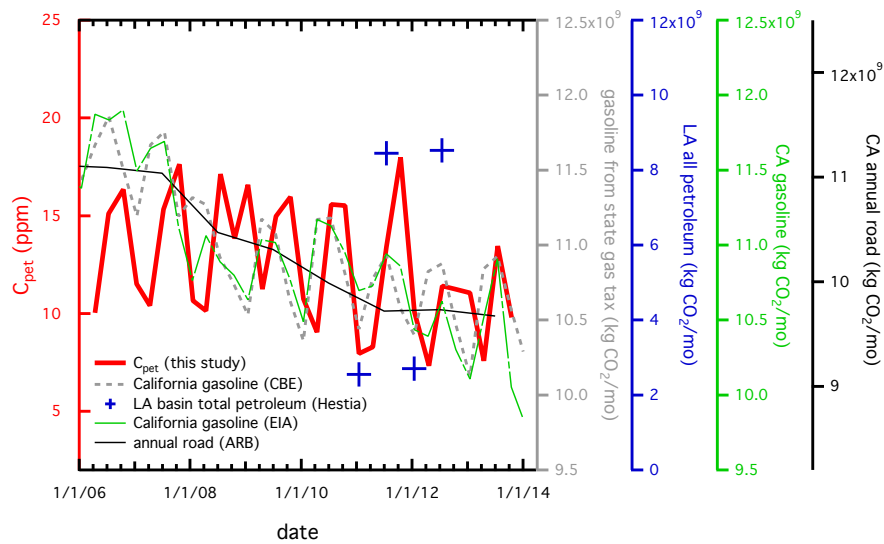


Figure 12. Comparison of the Pasadena  $C_{\text{pet}}$  atmospheric concentration with all available area-integrated bottom-up fossil fuel  $\text{CO}_2$  emissions **per month (mo)**, including gasoline sales based on taxes paid to the California Board of Equalization (CBE, 2014), gasoline provided in California by prime suppliers, the California Air Resources Board's annual road emissions (CARB, 2015), and the Hestia-LA gridded total petroleum. The Hestia-LA data product is specific to the Los Angeles megacity domain; all inventories are statewide estimates. Since the Hestia-LA product is gridded, we show the emissions emanating from different regions for January (northeast quadrant, Fig. 13a) and July (southwest quadrant), based on prevailing winds during those periods (Figs. 7 and 13a). The axis for each inventory has been adjusted to allow easy comparison. The seasonality of the  $C_{\text{pet}}$  data lags the bottom-up inventories by a few months. This analysis is consistent with the observed decrease in gasoline combustion during 2008-2011.

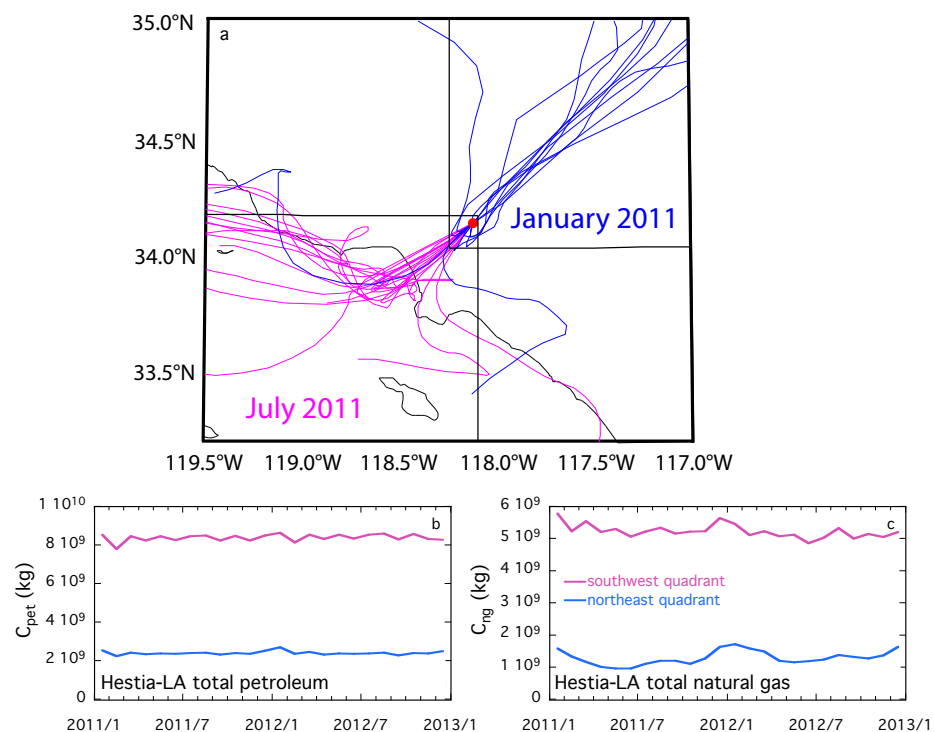


Figure 13. Relevant emissions selection from the Hestia-LA data product. (a) Quadrants selected for investigation of  $\text{CO}_2$  emissions from the Hestia-LA data product, together with the 24-hour back trajectories calculated by HYSPLIT for January (northeast quadrant) and July (southwest quadrant)  $\Delta^{14}\text{C}$  sampling days. The back trajectories end in Pasadena (red dot) at 1400 PST. Monthly averaged time series for Hestia-LA data product  $C_{\text{ff}}$  are shown from total petroleum combustion (b) and total natural gas combustion (c) for 2011 and 2012. For both the northeast quadrant of the Los Angeles region, the source of winter emissions, and the southwest quadrant, the source of summer emissions, the seasonal pattern is either flat (petroleum) or characterized by peaks during the winter (natural gas). But the summer emissions are always higher than those during winter, consistent with the observed top-down patterns for  $C_{\text{pet}}$  and  $C_{\text{ng}}$  in Pasadena.

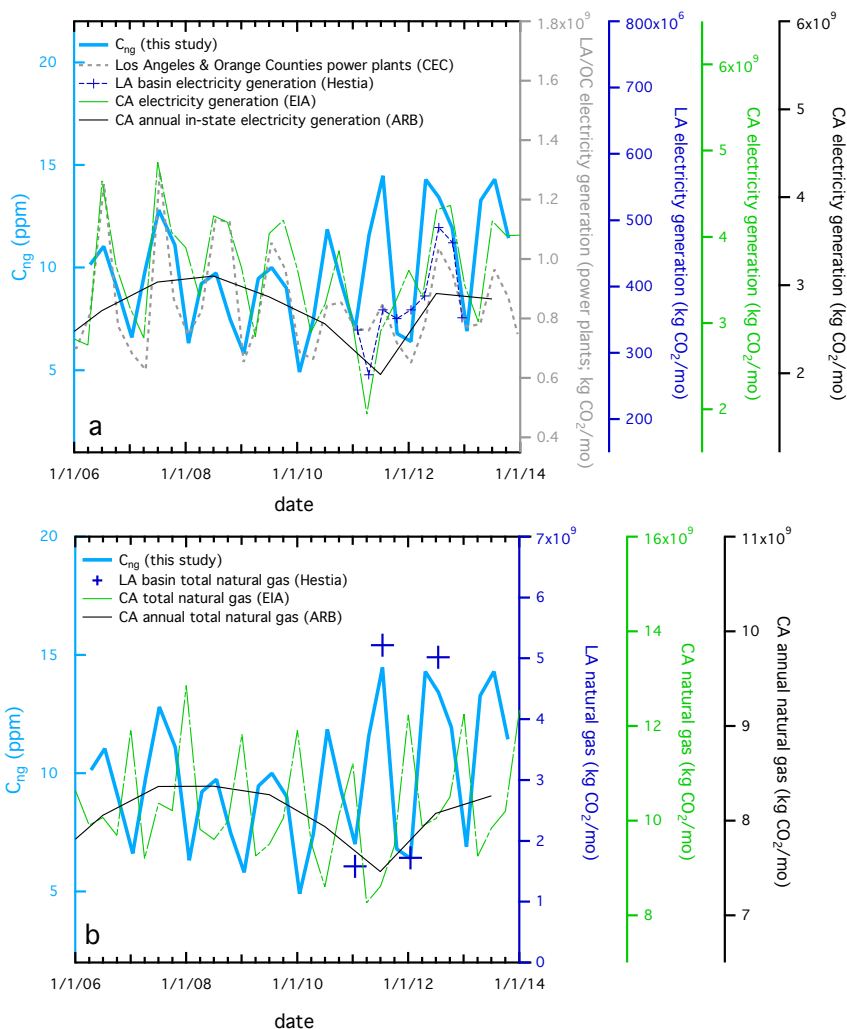
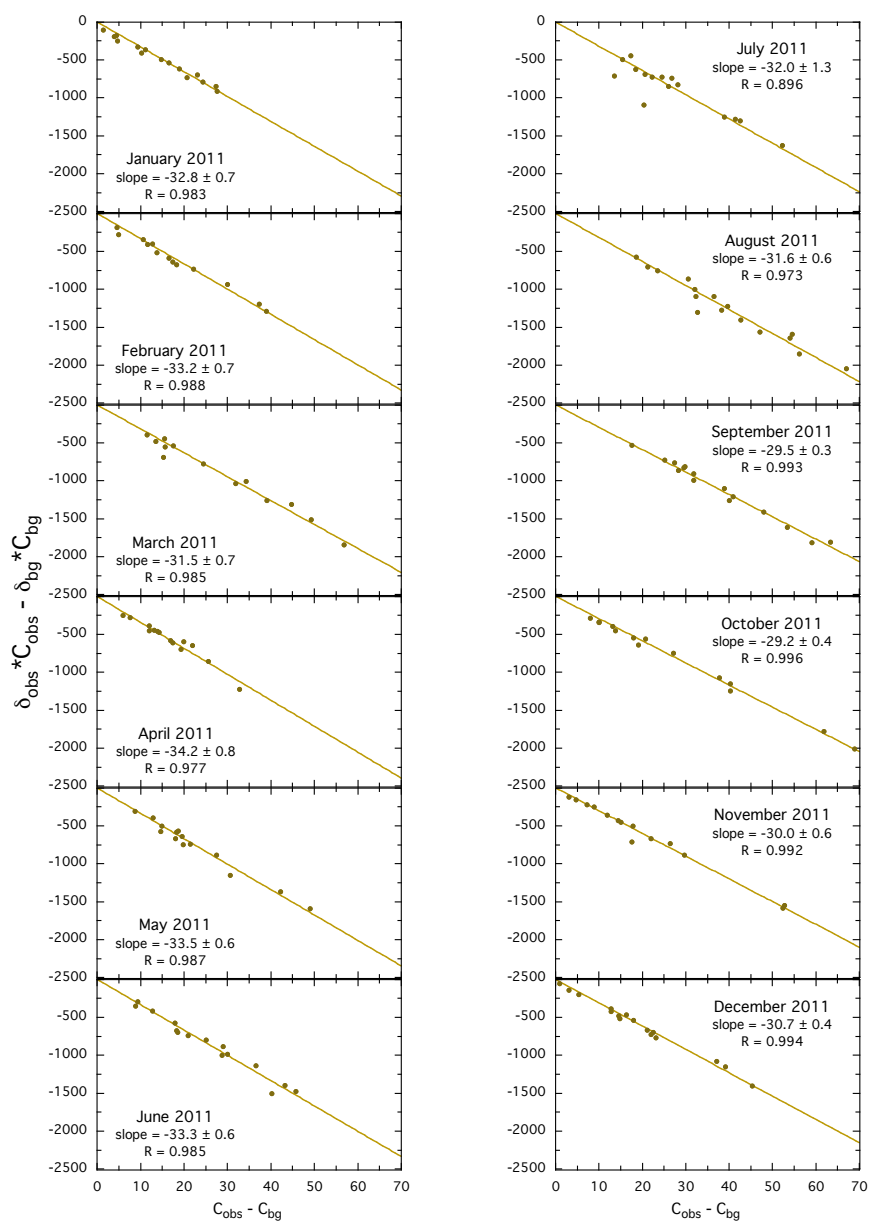


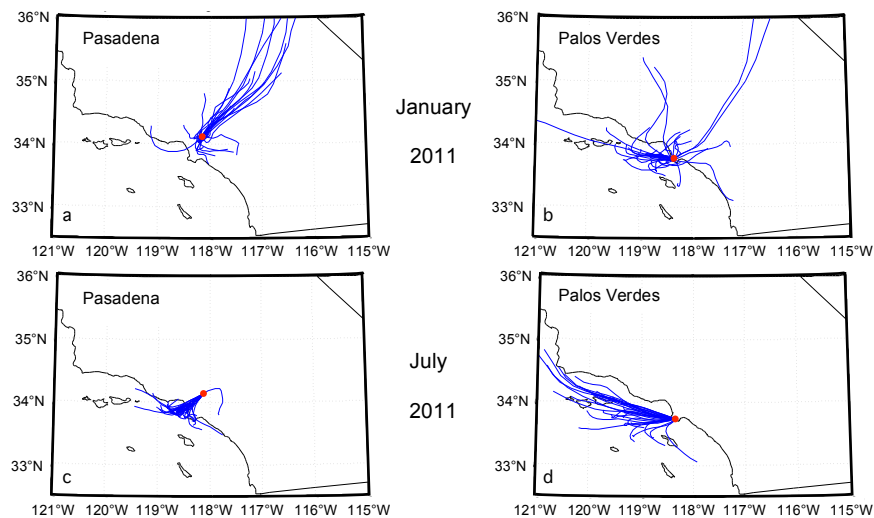
Figure 14. Comparison of Pasadena  $C_{ng}$  atmospheric concentration with area-integrated inventories of natural gas combustion, as well as the gridded Hestia-LA data product for southwest and northeast regional sectors for July and January months, respectively, in emissions/month (mo). Panel (a) compares the data from this paper with usage of natural gas by the electrical power sector; panel (b) shows the comparison with total natural gas consumption. Statewide inventories are given by EIA (2014) and CARB (2015) curves. Regional inventories include Hestia results and natural gas from power plants (CEC, 2014) in Los Angeles and Orange counties with monthly data (except Calabasas and Valencia). The vertical axes have been adjusted to allow easy comparison. This analysis is consistent with the increase in natural gas usage during the last few years.

1108 **Appendix**  
 1109 **1. Monthly Miller Tans plots for 2011**



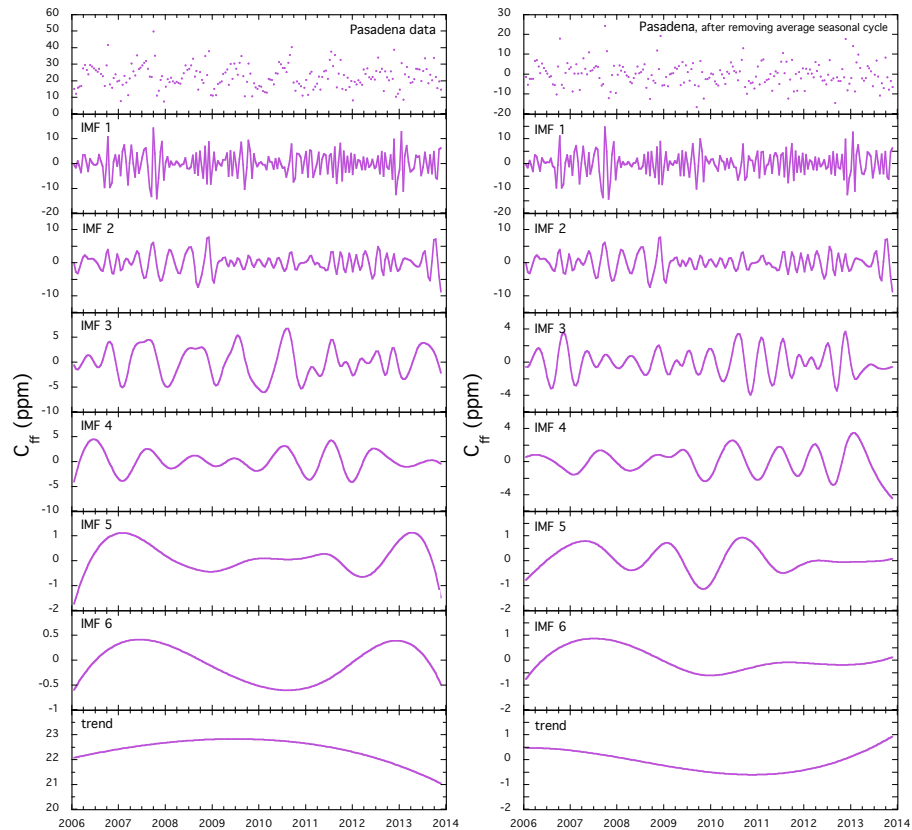
1110 Figure A1. Miller-Tans plots for each month in 2011. Values of the slopes for three-  
 1111 month seasonal averages are plotted in Fig. 6a.

1112    **2.    Back trajectories for both Pasadena and Palos Verdes sites**



1113    Figure A2. Twelve-hour back trajectories for all days in January and July, 2011, for the  
1114    Pasadena and Palos Verdes sites. This shows more detail for the effect of transport on the  
1115    air masses sampled during summer and winter at the Palos Verdes site than Fig. 7.

1116 **3. Full ensemble empirical mode decomposition results**



1117 Figure A3. Time series of all of the results from the ensemble empirical mode  
1118 decomposition (EEMD) analysis of the Pasadena  $C_{ff}$ . The left set of panels shows the  
1119 results for the raw data, whereas the right column shows those for the data after  
1120 subtraction of the average seasonal cycle. The long-term trend reflecting the economic  
1121 downturn of the Great Recession is reflected clearly in IMF 6 and the trend of the data  
1122 after the pronounced seasonality is removed (right-hand column), although there is some  
1123 evidence of it in IMF 6 of the raw  $C_{ff}$  data.